CENTRE DE RECERCA MATEMÀTICA

Title:	*Dynamics in a time-discrete food-chain model with strong pressure on preys*
Journal Information:	*Communications in Nonlinear Science and Numerical Simulation*,
Author(s):	Alsedà L., Vidiella B., Solé R., Lázaro J.T., Sardanyés J..
Volume, pages:	*84 1*, DOI:[10.1016/j.cnsns.2020.105187]

Commun Nonlinear Sci Numer Simulat 84 (2020) 105187

Contents lists available at ScienceDirect

Commun Nonlinear Sci Numer Simulat

journal homepage: www.elsevier.com/locate/cnsns

Research paper

Dynamics in a time-discrete food-chain model with strong pressure on preys☆

Ll. Alsedà[a,b,c,1], B. Vidiella[d,e,1], R. Solé[d,e,f], J.T. Lázaro[g,c], J. Sardanyés[b,c,*]

[a] Departament de Matemàtiques, Edifici C, Facultat de Ciències, Universitat Autònoma de Barcelona, Bellaterra, Barcelona 08193, Spain
[b] Centre de Recerca Matemàtica, Campus de Bellaterra, Edifici C, Bellaterra, Barcelona 08193, Spain
[c] Barcelona Graduate School of Mathematics (BGSMath), Campus de Bellaterra, Edifici C, Bellaterra, Barcelona 08193, Spain
[d] ICREA-Complex Systems Lab, Universitat Pompeu Fabra, Dr Aiguader 88, Barcelona 08003, Spain
[e] Institut de Biologia Evolutiva, CSIC-UPF, Pg Maritim de la Barceloneta 37, Barcelona 08003, Spain
[f] Santa Fe Institute, 1399 Hyde Park Road, Santa Fe NM 87501, USA
[g] Departament de Matemàtiques, Universitat Politècnica de Catalunya, Av. Diagonal, 647, Barcelona 08028, Spain

ARTICLE INFO

Article history:
Received 11 October 2019
Revised 20 December 2019
Accepted 12 January 2020
Available online 16 January 2020

Keywords:
Bifurcations
Chaos
Invariant sets
Mathematical ecology
Maps
Food chains

ABSTRACT

Discrete-time dynamics, mainly arising in boreal and temperate ecosystems for species with non-overlapping generations, have been largely studied to understand the dynamical outcomes due to changes in relevant ecological parameters. The local and global dynamical behaviour of many of these models is difficult to investigate analytically in the parameter space and, typically, numerical approaches are employed when the dimension of the phase space is large. In this article we provide topological and dynamical results for a map modelling a discrete-time, three-species food chain with two predator species interacting on the same prey. The domain where dynamics live is characterised, as well as the so-called escaping regions, which involve species extinctions. We also provide a full description of the local stability of equilibria within a volume of the parameter space given by the prey's growth rate and the predation rates. We have found that the increase of the pressure of predators on the prey results in chaos via a supercritical Neimark-Sacker bifurcation. Then, period-doubling bifurcations of invariant curves take place. Interestingly, an increasing predation directly on preys can shift the extinction of top predators to their survival, allowing an unstable persistence of the three species by means of periodic and chaotic attractors.

1. Introduction

Ecological systems display complex dynamical patterns both in space and time [1]. Although early work already pointed towards complex population fluctuations as an expected outcome of the nonlinear nature of species' interactions [2,3], the first evidences of chaos in species dynamics was not characterised until the late 1980's and 1990's [4,5]. Since pioneering works on one-dimensional discrete models [6–9] and on time-continuous ecological models, e.g., with the so-called spiral chaos [10,11] (already pointed out by Rössler in 1976 [12]), the field of ecological chaos experienced a strong debate and

☆ Dedicated to Mitchell Jay Feigenbaum, *in memoriam*.

* Corresponding author.
E-mail addresses: jose.tomas.lazaro@upc.edu (J.T. Lázaro), jsardanyes@crm.cat (J. Sardanyés).

[1] equal contribution

https://doi.org/10.1016/j.cnsns.2020.105187
1007-5704/

a rapid development [6,7,11,13–15], with several key papers offering a compelling evidence of chaotic dynamics in Nature, from vertebrate populations [13,16–20] to plankton dynamics [21] and insect species [4,5,22,23].

Discrete-time models have played a key role in the understanding of complex ecosystems, especially for those organisms undergoing one generation per year i.e., univoltine species [6,7,9]. The reason for that is the yearly forcing, which effectively makes the population emerging one year to be a discrete function of the population of the previous year [23]. These dynamics apply for different organisms such as insects in temperate and boreal climates. For instance, the speckled wood butterfly (*Pararge aegeria*) is univoltine in its most northern range. Adult butterflies emerge in late spring, mate, and die shortly after laying the eggs. Then, their offspring grow until pupation, entering diapause before winter. New adults emerge the following year thus resulting in a single generation of butterflies per year [24]. Hence, maps can properly represent the structure of species interactions and some studies have successfully provided experimental evidence for the proposed dynamics [4,5,22,23].

Further theoretical studies incorporating spatial dynamics strongly expanded the reach of chaotic behaviour as an expected outcome of discrete population dynamics [25,26]. Similarly, models incorporating evolutionary dynamics and mutational exploration of genotypes easily lead to chaotic attractors in continuous [27] and discrete [28] time. The so-called *homeochaos* has been identified in discrete multi-species models with victim-exploiter dynamics [29,30].

The dynamical richness of discrete ecological models was early recognised [6–8,31] and special attention has been paid to food chains incorporating three species in both continuous [11,32–36] and discrete [37–39] time systems. In this paper we address this problem by using a simple trophic model of three species interactions that generalises a previous two-dimensional predator-prey model, given by the difference Equations (4.5) in [40] (see also [41]). The two-dimensional model assumes a food chain structure with an upper limit to the total population of preys, whose growth rate is affected by a single predator. The new three-dimensional model explored in this article introduces a new top predator species that consumes the predator and interferes in the growth of the preys.

We provide a full description of the local dynamics and the bifurcations in a wide region of the three-dimensional parameter space containing relevant ecological dynamics. This parameter cuboid is built using the prey's growth rates and the two predation rates as axes. The first predation rate concerns to the predator that consumes the preys, while the second predator rate is the consumption of the first predator species by the top predator. As we will show, this model displays remarkable examples of chaotic attractors. The route to chaos associated to increasing predation strengths are shown to be given by period-doubling bifurcations of invariant curves, which arise via a supercritical Neimark-Sacker bifurcation.

Some of the analyses of this paper are complemented, as supplementary material, with 6 movies.

2. Three species predator-prey map

Discrete-time dynamical systems are appropriate for describing the population dynamics of species with non-overlapping generations [4,6,7,24,42]. Such species are found in temperate and boreal regions because of their seasonal environments. We here consider a food chain of three interacting species, each with non-overlapping generations. We specifically consider a population of preys x which is predated by a first predator with population y. We also consider a third species given by a top predator z that predates on the first predator y, also interfering in the growth of prey's population according to Fig. 1. Examples of top-predator → predator → prey interactions in univoltine populations can be found in ecosystems. For instance, the heteroptera species *Picromerus bidens* in northern Scandinavia [43], which predates the butterfly *Pararge aegeria* by consuming on its eggs. Other species, such as spiders, can also act as top-predators (e.g., genus *Clubiona sp.*, with a wide distribution in northern Europe and Greenland).

The next set of difference equations aims at modelling the three-species food chain displayed in Fig. 1. This is a very simple model incorporating a minimum number of parameters that ease its analytical tractability. Despite other discrete time models have been employed to investigate dynamics of insects in experimental settings [4,5], our approach is purely

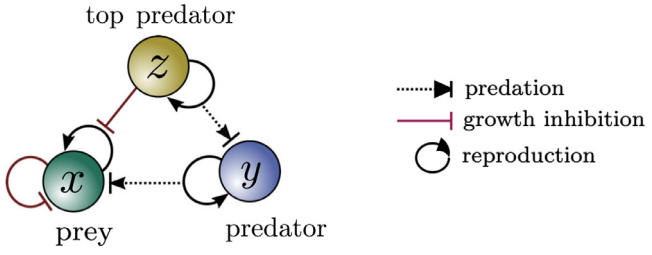

Fig. 1. Schematic diagram of the investigated dynamical system formed by a prey, a predator, and a top-predator. The diagram displays the ecological interactions modelled with Map (1), given by predation (dashed arrow), growth inhibition (e.g., competition, red lines), and reproduction (closed arrows).

qualitative. This simple food chain can be described by the following system of nonlinear difference equations:

$$\begin{pmatrix} x_{n+1} \\ y_{n+1} \\ z_{n+1} \end{pmatrix} = T \begin{pmatrix} x_n \\ y_n \\ z_n \end{pmatrix} \text{ where } T \begin{pmatrix} x \\ y \\ z \end{pmatrix} = \begin{pmatrix} \mu x(1-x-y-z) \\ \beta y(x-z) \\ \gamma yz \end{pmatrix} \tag{1}$$

where x, y, z denote population densities with respect to a normalised carrying capacity ($K = 1$). We note that populations densities need to be non-negative to be biologically-meaningful.

Constants μ, β, γ are positive. In the absence of predation, as mentioned, preys grow logistically (with intra-specific competition) with an intrinsic reproduction rate μ. However, preys' reproduction is decreased by the action of predation from both predators y and z. The effective growth rate of predators y is β. Finally, γ is the growth rate of predators z due to the consumption of species y. Notice that predator z also predates (interferes) on x, but it is assumed that the increase in reproduction of the top predator z is mainly given by the consumption of species y. Model (1) is defined on the phase space, given by the simplex

$$\mathbb{U} := \left\{(x, y, z) \in \mathbb{R}^3 \, : x, y, z \geq 0 \text{ and } x + y + z \leq 1\right\}$$

and, although it is meaningful for the parameters' set

$$\left\{(\mu, \beta, \gamma) \in \mathbb{R}^3 \, : \mu > 0, \ \beta > 0 \text{ and } \gamma > 0\right\}$$

of all positive parameters, we will restrict ourselves to the following particular cuboid

$$\mathrm{Q} = \{(\mu, \beta, \gamma) \in (0, 4] \times [2.5, 5] \times [5, 9.4]\} \tag{2}$$

which exhibits relevant biological dynamics (in particular bifurcations and routes to chaos).

The next proposition lists some very simple dynamical facts about System (1) on the domain $\mathbb{U}$ with parameters in the cuboid Q. It is a first approximation to the understanding of the dynamics of this system.

A set $A \subset \mathbb{U}$ is called *T-invariant* whenever $T(A) \subset A$.

Proposition 1. *The following statements hold for System (1) and all parameters* $(\mu, \beta, \gamma) \in \mathrm{Q}$.

(a) *The point* $(0, 0, 0) \in \mathbb{U}$ *is a fixed point of T which corresponds to extinction of the three species.*
(b) $T(\{(1, 0, 0)\}) = T(\{(0, y, 0) \in \mathbb{U}\}) = T(\{(0, 0, z) \in \mathbb{U}\}) = (0, 0, 0)$. *That is, the point (1,0,0) and every initial condition in* $\mathbb{U}$ *on the y and z axes lead to extinction in one iterate.*
(c) $T(\{(x, 0, z) \in \mathbb{U}\}) \subset \{(x, 0, 0) \in \mathbb{U}\} \subset \{(x, 0, z) \in \mathbb{U}\}$. *In particular the sets* $\{(x, 0, z) \in \mathbb{U}\}$ *and* $\{(x, 0, 0) \in \mathbb{U}\}$ *are T-invariant.*

Proof. Statements (a) and (b) follow straightforwardly. To prove (c) notice that $T((x, 0, z)) = (\mu x(1 - x - z), 0, 0)$ with $\mu \in (0, 4]$, $x \geq 0$ and $x + z \leq 1$. Hence,

$$0 \leq \mu x(1 - x - z) = \mu x(1 - x) - \mu xz \leq 1 - \mu xz \leq 1,$$

and thus $(\mu x(1 - x - z), 0, 0) \in \mathbb{U}$. □

An important natural question is: what is the (maximal) subset $\mathcal{S}$ of $\mathbb{U}$ where the Dynamical System associated to Model (1) is well defined for all iterates (i.e. $T^n(x, y, z) \in \mathbb{U}$ for every $n \in \mathbb{N}$ and $(x, y, z) \in \mathcal{S}$). Such a set is called the *invariant set* of System (1). The domain $\mathcal{S}$ has a complicated geometry and is difficult to characterise (see Fig. 2).

To get a, perhaps simpler, definition of the *invariant set* $\mathcal{S}$ and to study the different scenarios leading to extinctions, we introduce the *one-step escaping set* $\Theta = \Theta(\mu, \beta, \gamma)$ of System (1) defined as the set of points $(x, y, z) \in \mathbb{U}$ such that $T(x, y, z) \notin \mathbb{U}$, and the *escaping set* $\Gamma = \Gamma(\mu, \beta, \gamma)$ as the set of points $(x, y, z) \in \mathbb{U}$ such that $T^n(x, y, z) \notin \mathbb{U}$ for some $n \geq 1$. Clearly,

$$\Gamma = \mathbb{U} \cap \left(\bigcup_{n=0}^{\infty} T^{-n}(\Theta) \right).$$

We must notice that the escaping set Γ contains initial conditions of the phase space whose orbit, after some iterates, gets out of the domain $\mathbb{U}$ of System (1). This can be achieved in two different ways: (i) the carrying capacity is surpassed, i.e., $x + y + z > 1$; and (ii) the variable y becomes negative (this happens if and only if, in the previous iterate, $z > x$). In both cases, from a purely mathematical point of view, the orbits can not be iterated anymore because the orbit is out of the domain of definition of the Map (1). However, from a biological perspective we note that after the orbit leaves the domain, extinctions take place (i.e., solutions will rapidly become negative). For Phenomenon (i), the surpass of the carrying capacity causes an immediate cascade of extinctions of the three species after (very) few more iterates (see Fig. 3). Indeed, once the carrying capacity is overcome, the prey becomes extinct and so do predators y and z consecutively. Phenomenon (ii) involves the extinction of the two predator species (first predator y and top predator at the next iterate), and the dynamics is then governed by the logistic map for preys x. As shown below, these escaping regions belong to a highly complex (apparently fractal) set.

An example of the escaping set Γ (setting $z_0 = 0$ for the sake of a clear visualisation) is illustrated in Fig. 3 (see also Movie-1.mp4 to visualise how the escaping sets change with the parameters in the space (x, y, z)). Specifically, the different colours in the spaces (x, y) indicate the number of iterates (here showing from 1 to 50) needed to leave the domain

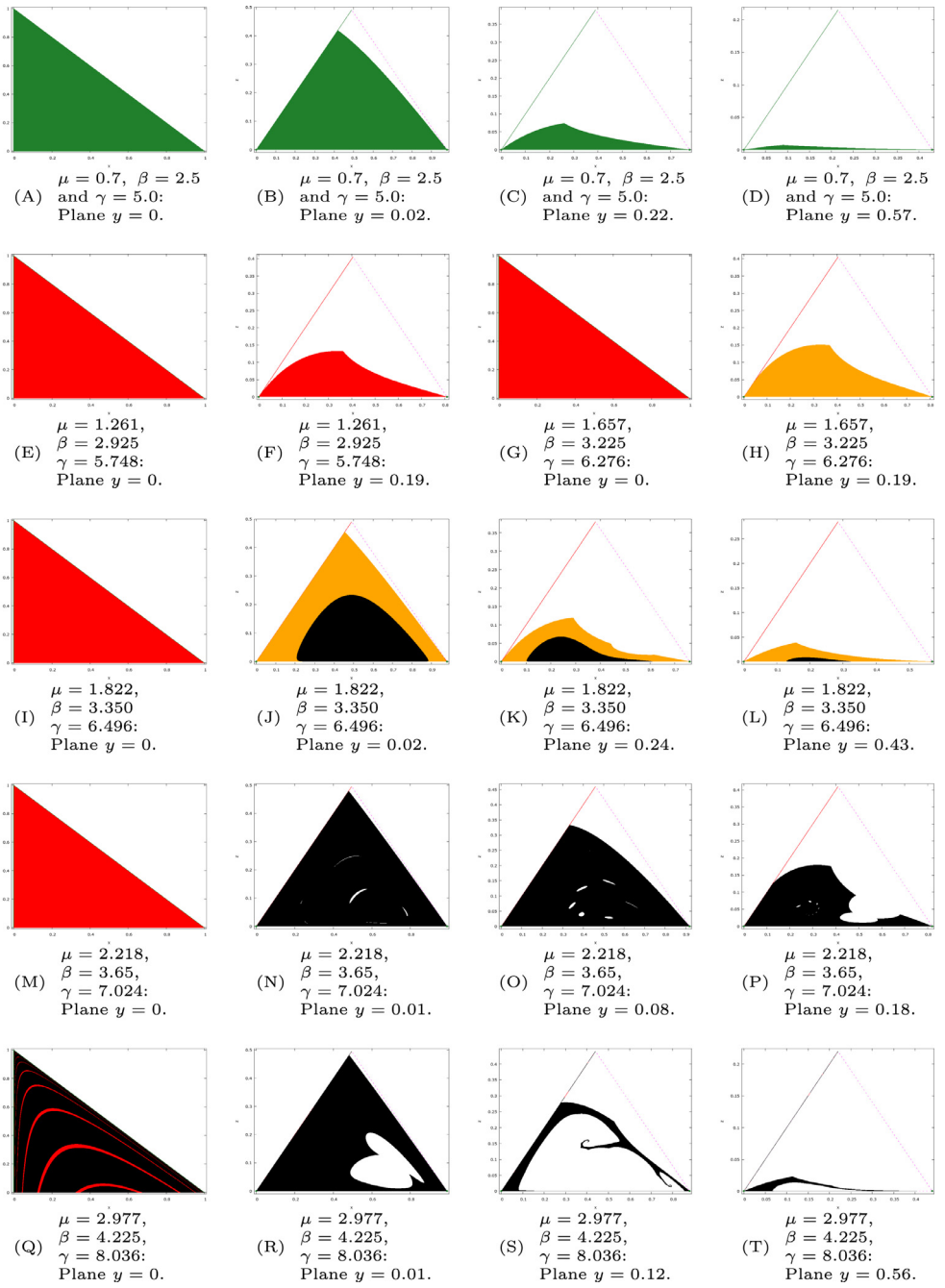

Fig. 2. Plots of the intersection of $\mathcal{S}$ with the planes $y = \text{ctnt}$ for several choices of the planes and the parameters μ, β and γ. Points drawn in dark green color converge to the fixed point (0,0,0), points in red converge to the fixed point $(\frac{\mu-1}{\mu}, 0, 0)$, points in orange converge to the fixed point $(\beta^{-1}, 1-\mu^{-1}-\beta^{-1}, 0)$, and points in black belong to the invariant set $\mathcal{S}$ but do not belong to the basin of attraction of any fixed point. The dashed magenta lines show the boundary of the cut of the plane $y = \text{ctnt}$ with the domain $\mathcal{E}$ (which is defined in page 7).

$\mathcal{S}$ (in this case we have chosen initial conditions and parameter values involving the surpass of the carrying capacity, i.e., Phenomenon (i)). The time series show that, after an irregular dynamics, both preys and predator y become suddenly extinct, as indicated by the vertical rectangles at the end of the time series. We want to emphasise that these extinctions are due to the discrete nature of *time*. That is, they have nothing to do with the ω-limit sets of the dynamical system. Similar phenomena are found in the full simplex with an initial presence of all the species. On the other hand, concerning Phenomenon (ii), Table 1 shows (as an example) some approximate iterates of the point $(x_0, y_0, z_0) = (0.72, 0.03, 0.003)$ for $(\mu, \beta, \gamma) = (3.43, 4, 7)$. Observe that all these iterates belong to $\mathbb{U}$ because $x_n,\ y_n,\ z_n > 0$ and $x_n + y_n + z_n < 1$. However,

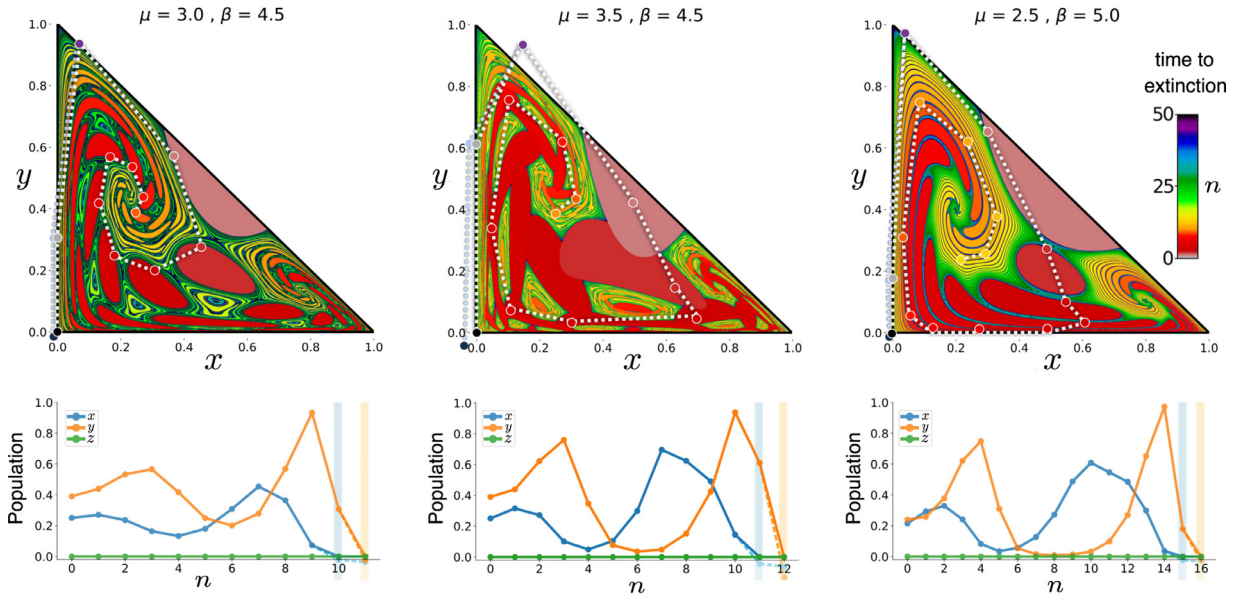

Fig. 3. (Upper) Escaping sets, Γ, obtained by iteration for parameter values giving place to complex (fractal) shapes, computed on the phase plane $z = 0$. The colours display the time that a given orbit overcomes the carrying capacity then going to extinction (colour gradient indicates the number of iterations to extinction, from 1 (pink) to 50 (violet) iterations). The small circles connected by the dashed white line indicate how iterates move from the initial condition $(x_0, y_0, z_0) = (0.25, 0.39, 0)$ towards extinction. (Bottom) Extinction time series for preys and predators, y. From left to right: $(x_0, y_0, z_0) = (0.25, 0.39, 0)$ and $(\mu, \beta, \gamma) = (3.0, 4.5, 7.5)$; $(x_0, y_0, z_0) = (0.25, 0.39, 0)$ and $(\mu, \beta, \gamma) = (3.5, 4.5, 7.5)$; and $(x_0, y_0, z_0) = (0.215, 0.24, 0)$ and $(\mu, \beta, \gamma) = (2.5, 5, 7.5)$. Vertical bars indicate when iterates for x and y become negative after surpassing the carrying capacity (For interpretation of the references to colour in this figure legend, the reader is referred to the web version of this article.).

Table 1
Approximate iterates of the point $(x_0, y_0, z_0) = (0.72, 0.03, 0.003)$ for $(\mu, \beta, \gamma) = (3.43, 4, 7)$.

n	(x_n, y_n, z_n)	$x_n + y_n + z_n$	$x_n - z_n$
0	(0.72,0.03,0.003)	0.753	0.717
1	(0.6099912,0.0860400,0.0006300)	0.6966612	0.6093612
2	(0.6346666,0.2097178,0.0003794)	0.8447638	0.6342872
3	(0.3379347,0.5320851,0.0005570)	0.8705768	0.3373777
4	(0.1500165,0.7180545,0.0020747)	0.8701457	0.1479418
5	(0.0668174,0.4249211,0.0104281)	0.5021666	0.0563892
6	(0.1140953,0.0958439,0.0310180)	0.2409571	0.0830773
7	(0.2970489,0.0318498,0.0208102)	0.3497089	0.2762388
8	(0.6625672,0.0351926,0.0046396)	0.7023994	0.6579276
9	(0.6763288,0.0926168,0.0011430)	0.7700885	0.6751858
10	(0.5333505,0.2501341,0.0007410)	0.7842256	0.5326095
11	(0.3947360,0.5328952,0.0012974)	0.9289286	0.3934386
12	(0.0962267,0.8386461,0.0048398)	0.9397126	0.0913869
13	(0.0198983,0.3065650,0.0284122)	0.3548755	-0.0085139

since $x_{13} - z_{13} < 0$, we have $y_{14} < 0$ which implies the extinction of predator y which in turn implies the extinction of predator z in the iterate 15.

The *invariant set* of System (1) can also be defined as:

$$\mathcal{S} := \mathbb{U} \setminus \Gamma = \mathbb{U} \setminus \bigcup_{n=0}^{\infty} T^{-n}(\Theta).$$

In general we have $\Gamma \supset \Theta \neq \emptyset$ and, hence, $\mathcal{S} \subsetneq \mathbb{U}$ (that is, $\mathbb{U}$ may not be the invariant set of System (1)). On the other hand, for every μ, β, $\gamma > 0$, $\mathcal{S}$ is non-empty (it contains at least the point (0,0,0)) and T-invariant. Moreover, since the map T is (clearly) non-invertible, a backward orbit of a point from $\mathcal{S}$ is not uniquely defined.

As we have pointed out, the domain $\mathcal{S}$ is geometrically complicated and of difficult characterisation. However, despite of the fact that this knowledge is important for the understanding of the global dynamics, in this paper we will omit this challenging study and we will consider System (1) on the domain

$$\mathcal{E} = \{(x, 0, z) \in \mathbb{U}\} \cup \{(x, y, z) \in \mathbb{U} : y > 0 \text{ and } x \geq z\}.$$

(see Fig. 4) which is an approximation of $\mathcal{S}$ better than $\mathbb{U}$, as stated in the next proposition.

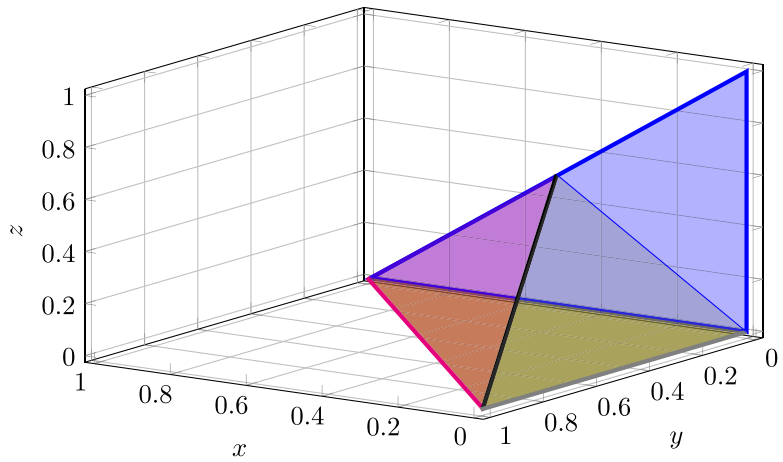

Fig. 4. Plot of the domain $\mathcal{E}$. The "wall" $y = 0$: $\{(x, 0, z) \in \mathbb{U}\}$ is drawn in blue. The face $z = 0$: $\{(x, y, 0) \in \mathbb{U}\}$ is drawn in olive color; The face $x + y + z = 1$: $\{(x, y, z) \in \mathbb{U} : y > 0,\ x \geq z \text{ and } x + y + z = 1\}$ in magenta, and the face $x = z$: $\{(x, y, x) \in \mathbb{U} : y > 0\}$ in gray.

Proposition 2. *For System (1) and all parameters* $(\mu, \beta, \gamma) \in \mathsf{Q}$ *we have*

$$\{(x, 0, z) \in \mathbb{U}\} \cup \{(0, y, 0) \in \mathbb{U}\} \subset \mathcal{S} \subset \mathcal{E}.$$

Proof. The fact that $\{(x, 0, z) \in \mathbb{U}\} \cup \{(0, y, 0) \in \mathbb{U}\} \subset \mathcal{S}$ follows directly from Proposition 1. To prove the other inclusion observe that

$$\mathcal{E} = \mathbb{U} \setminus \{(x, y, z) \in \mathbb{U} : y > 0 \text{ and } z > x\},$$

and for every $(x, y, z) \in \mathbb{U}$ with $y > 0$ and $z > x$ we have $\beta y(x - z) < 0$ because $\beta > 0$. Consequently, $\{(x, y, z) \in \mathbb{U} : y > 0 \text{ and } z > x\} \subset \Theta$, and hence,

$$\mathcal{S} = \mathbb{U} \setminus \bigcup_{n=0}^{\infty} T^{-n}(\Theta) \subset \mathbb{U} \setminus \Theta \subset \mathbb{U} \setminus \{(x, y, z) \in \mathbb{U} : y > 0 \text{ and } z > x\} = \mathcal{E}.$$

□

Remark 3. If a periodic orbit is contained in the set $\mathbb{U}$ it is automatically contained in the set $\mathcal{S}$, and by Proposition 2 it is also contained in $\mathcal{E}$.

3. Fixed points and local stability

This section is devoted to compute the biologically-meaningful fixed points of T in $\mathcal{E}$, and to analyse their local stability. This study will be carried out in terms of the positive parameters μ, β, γ.

The dynamical system defined by (1) has the following four (biologically meaningful) fixed points in the domain $\mathcal{E}$ (see Fig. 5):

$$P_1^* = (0, 0, 0),$$
$$P_2^* = \left(\frac{\mu - 1}{\mu}, 0, 0\right),$$
$$P_3^* = \left(\frac{1}{\beta}, 1 - \frac{1}{\mu} - \frac{1}{\beta}, 0\right),$$
$$P_4^* = \left(\frac{1}{2}\left(1 - \mu^{-1} + \beta^{-1} - \gamma^{-1}\right), \frac{1}{\gamma}, \frac{1}{2}\left(1 - \mu^{-1} - \beta^{-1} - \gamma^{-1}\right)\right).$$

Notice that the system admits a fifth fixed point $P_5^* = (0, \frac{1}{\gamma}, -\frac{1}{\beta})$, which is not biologically meaningful since it has a negative coordinate (recall that $\beta > 0$), and thus it will not be taken into account in this study.

The fixed points P_1^*, P_2^*, and P_3^* are boundary equilibria, while P_4^* is a boundary equilibrium if $\mu^{-1} + \beta^{-1} + \gamma^{-1} = 1$ and interior otherwise. The fixed point P_1^* is the origin, representing the extinction of all the species. P_2^* is a boundary fixed point, with absence of the two predator species. The point P_3^* is the boundary fixed point in the absence of the top-level predator $z = 0$, while the point P_4^*, when it is located in the interior of $\mathcal{E}$, corresponds to a coexistence equilibrium.

The next lemma gives necessary and sufficient conditions for the fixed points P_1^*, P_2^*, P_3^*, and P_4^* to be biologically meaningful (belong to the domain $\mathbb{U}$ and, hence, to $\mathcal{E}$ — see, for instance, Fig. 5 and Movie-2.avi; see also the right part of Fig. 6).

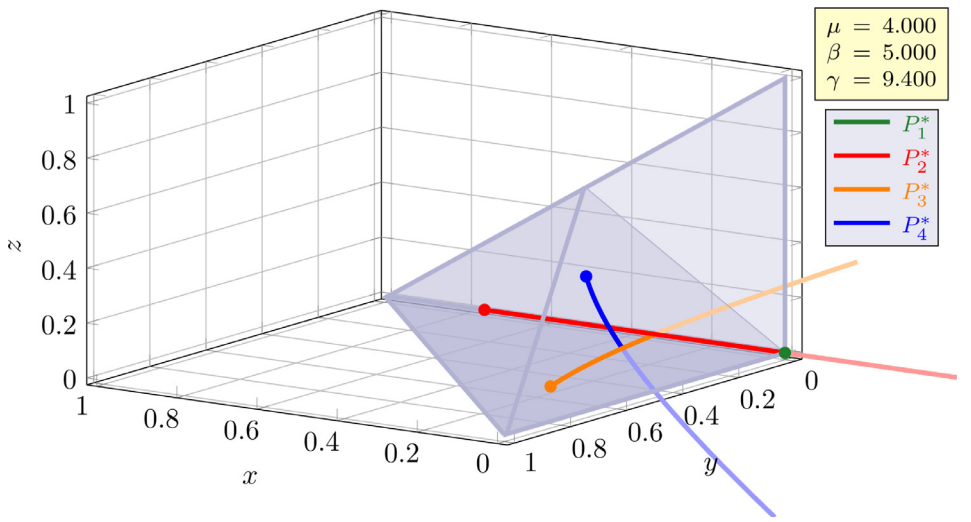

Fig. 5. The fixed point P_1^* in dark green color and the paths described by P_2^* in red, P_3^* in orange and P_4^* in blue in the domain $\mathcal{E}$ (plotted in violet) when the parameters $(\mu,\ \beta,\ \gamma)$ follow the path $(\mu(t), \beta(t), \gamma(t)) = (3.3, 2.5, 4.4)t + (0.7, 2.5, 5)$ with t ranging from 0 to 1. The pieces of the paths outside the domain $\mathcal{E}$, which correspond to non-biologically meaningful situations, are drawn with the soften color. The path described by the fixed point P_2^* in $\mathcal{E}$ bifurcates from P_1^* when $\mu = 1$. The path described by P_3^* in $\mathcal{E}$ bifurcates from P_2^* when $\mu = \frac{\beta}{\beta-1}$. The path of P_4^* in $\mathcal{E}$ bifurcates from P_3^* when $\mu^{-1} + \beta^{-1} + \gamma^{-1} = 1$ (or, equivalently, when $\mu = \frac{\beta\gamma}{(\beta-1)\gamma-\beta}$).

Lemma 4. *The following statements hold for every parameters' choice* $(\mu, \beta, \gamma) \in \mathsf{Q}$:

- $\boldsymbol{P_1^*}$: *The fixed point* P_1^* *belongs to* $\mathcal{E}$.
- $\boldsymbol{P_2^*}$:*The fixed point* P_2^* *belongs to* $\mathcal{E}$ *if and only if* $\mu \geq 1$. *Moreover,* $P_2^* = P_1^*$ *if and only if* $\mu = 1$.
- $\boldsymbol{P_3^*}$:*The fixed point* P_3^* *belongs to* $\mathcal{E}$ *if and only if* $\mu \geq \frac{\beta}{\beta-1} \geq \frac{5}{4}$ *(which is equivalent to* $\frac{1}{\mu} + \frac{1}{\beta} \leq 1$ *and* $\beta \leq 5$*). Moreover,* $P_3^* = P_2^*$ *if and only if* $\mu = \frac{\beta}{\beta-1}$.
- $\boldsymbol{P_4^*}$: *The fixed point* P_4^* *belongs to* $\mathcal{E}$ *if and only if* $\mu^{-1} + \beta^{-1} + \gamma^{-1} \leq 1$ *(which is equivalent to* $\mu \geq \frac{\beta\gamma}{(\beta-1)\gamma-\beta}$*). Moreover,* $P_4^* = P_3^*$ *if and only if* $\mu^{-1} + \beta^{-1} + \gamma^{-1} = 1$.

Proof. The statements concerning P_1^* and P_2^* follow straightforwardly from their formulae (see also Fig. 5) since, for $\mu \geq 1$, $\frac{\mu-1}{\mu} \in [0, \frac{3}{4}]$.

For the fixed point P_3^* when $\frac{1}{\mu} + \frac{1}{\beta} \leq 1$ we have $0 < \frac{1}{\beta}$,$0 \leq 1 - \frac{1}{\mu} - \frac{1}{\beta}$, and $\frac{1}{\beta} + (1 - \frac{1}{\mu} - \frac{1}{\beta}) = 1 - \frac{1}{\mu} < 1$. So,

$$P_3^* \in \left\{(x, y, 0) \in \mathbb{R}^3 : x, y \geq 0 \text{ and } x + y \leq 1\right\} \subset \{(x, y, 0) \in \mathcal{E}\} \subset \mathcal{E}.$$

Moreover, when $\frac{1}{\mu} + \frac{1}{\beta} = 1$ we have

$$P_3^* = \left(\frac{1}{\beta}, 1 - \frac{1}{\mu} - \frac{1}{\beta}, 0\right) = \left(1 - \frac{1}{\mu}, 0, 0\right) = P_2^*.$$

For the fixed point $P_4^* = (\frac{1}{2}(1 - \mu^{-1} + \beta^{-1} - \gamma^{-1}), \frac{1}{\gamma}, \frac{1}{2}(1 - \mu^{-1} - \beta^{-1} - \gamma^{-1}))$ when $\mu^{-1} + \beta^{-1} + \gamma^{-1} \leq 1$ we have

$$0 < \frac{1}{\gamma},$$

$$0 \leq \frac{1}{2}\left(1 - \mu^{-1} - \beta^{-1} - \gamma^{-1}\right),$$

$$0 < \beta^{-1} \leq \frac{1}{2}\left(1 - \mu^{-1} + \beta^{-1} - \gamma^{-1}\right), \text{ and}$$

$$\frac{1}{2}\left(1 - \mu^{-1} + \beta^{-1} - \gamma^{-1}\right) + \frac{1}{\gamma} + \frac{1}{2}\left(1 - \mu^{-1} - \beta^{-1} - \gamma^{-1}\right) = 1 - \frac{1}{\mu} < 1.$$

So,

$$P_4^* \in \{(x, y, z) \in \mathbb{U} : y > 0 \text{ and } x \geq z\} \subset \mathcal{E}.$$

Moreover, when $\mu^{-1} + \beta^{-1} + \gamma^{-1} = 1$ (that is, $1 - \mu^{-1} - \beta^{-1} - \gamma^{-1} = 0$) we have

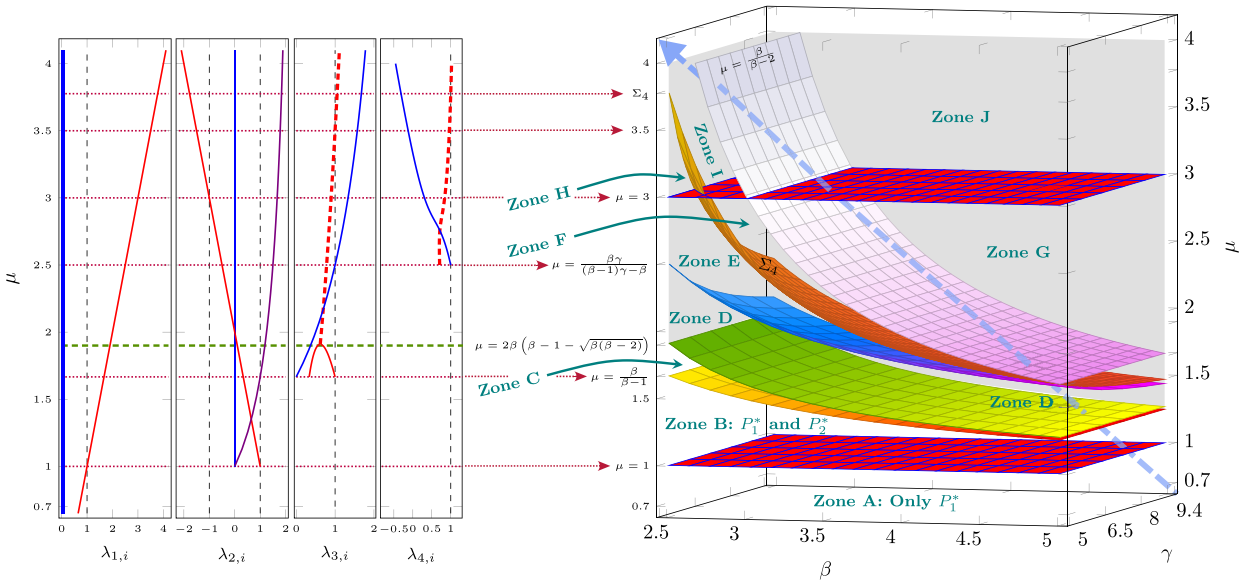

Fig. 6. (Left) Eigenvalues $\lambda_{j,i}$ of the fixed points P_j^*, with $j = 1, \ldots, 4$ and $i = 1, \ldots, 3$ (for typical values of β and γ). (Right) Zones of local structural stability in the parameter space. The blue, reddish, and violet surfaces intersect at the unique point $\left(5, 5, \frac{5}{3}\right)$. For every other value of $(\beta, \gamma) \in [2.5, 5] \times [5, 9.4]$ are pairwise disjoint. The grey box above the surface $\mu = 2\beta\left(\beta - 1 - \sqrt{\beta(\beta-2)}\right)$ is the region where the eigenvalues $\lambda_{3,2}$ and $\lambda_{3,3}$ are complex. The eigenvalues $\lambda_{4,2}$ and $\lambda_{4,3}$ are complex whenever P_4^* is in the positive octant. The red thick dashed lines (left) represent $|\lambda_{3,2}| = |\lambda_{3,3}|$ and $|\lambda_{4,2}| = |\lambda_{4,3}|$. In the left pictures the "complexity region" of $\lambda_{3,2}$ and $\lambda_{3,3}$ corresponds to the values of μ above the green thick dashed line. The dynamics tied to the zones crossed by the thick, dashed, blue arrow is shown in Movie-3.mp4.

$$\gamma^{-1} = 1 - \mu^{-1} - \beta^{-1}, \text{ and}$$
$$1 - \mu^{-1} + \beta^{-1} - \gamma^{-1} = 1 - \mu^{-1} - \beta^{-1} - \gamma^{-1} + 2\beta^{-1} = 2\beta^{-1}.$$

Consequently,

$$P_4^* = \left(\frac{1}{2}\left(1 - \mu^{-1} + \beta^{-1} - \gamma^{-1}\right), \frac{1}{\gamma}, \frac{1}{2}\left(1 - \mu^{-1} - \beta^{-1} - \gamma^{-1}\right)\right)$$
$$= \left(\beta^{-1}, 1 - \mu^{-1} - \beta^{-1}, 0\right) = P_3^*.$$

□

Henceforth, this section will be devoted to the study of the local stability and dynamics around the fixed points $P_1^*, \ldots, P_4^*$ for parameters moving in Q. This work is carried out by means of four lemmas (Lemmas 5–8). The information provided by them is summarised graphically in Figs. 6 and 7.

The study of the stability around the fixed points is based on the computation of the eigenvalues of its Jacobian matrix. In our case, the Jacobian matrix of map (1) at a point (x, y, z) is

$$J(x, y, z) = \begin{pmatrix} \mu(1 - 2x - y - z) & -\mu x & -\mu x \\ \beta y & \beta(x - z) & -\beta y \\ 0 & \gamma z & \gamma y \end{pmatrix}$$

and has determinant $\det(J(x, y, z)) = \mu\beta\gamma xy(1 - 2x - 2z)$.

The first one of these lemmas follows from a really simple computation.

Lemma 5. *The point $P_1^* = (0, 0, 0)$ is a boundary fixed point of System (1) for any positive μ, β, γ. Moreover, P_1^* is:*

- *non-hyperbolic when $\mu = 1$,*
- *a locally asymptotically stable sink node when $0 < \mu < 1$, and*
- *a saddle with an unstable invariant manifold of dimension 1, locally tangent to the x-axis, when $\mu > 1$.*

Proof. The Jacobian matrix of System (1) at P_1^* is

$$J(P_1^*) = \begin{pmatrix} \mu & 0 & 0 \\ 0 & 0 & 0 \\ 0 & 0 & 0 \end{pmatrix},$$

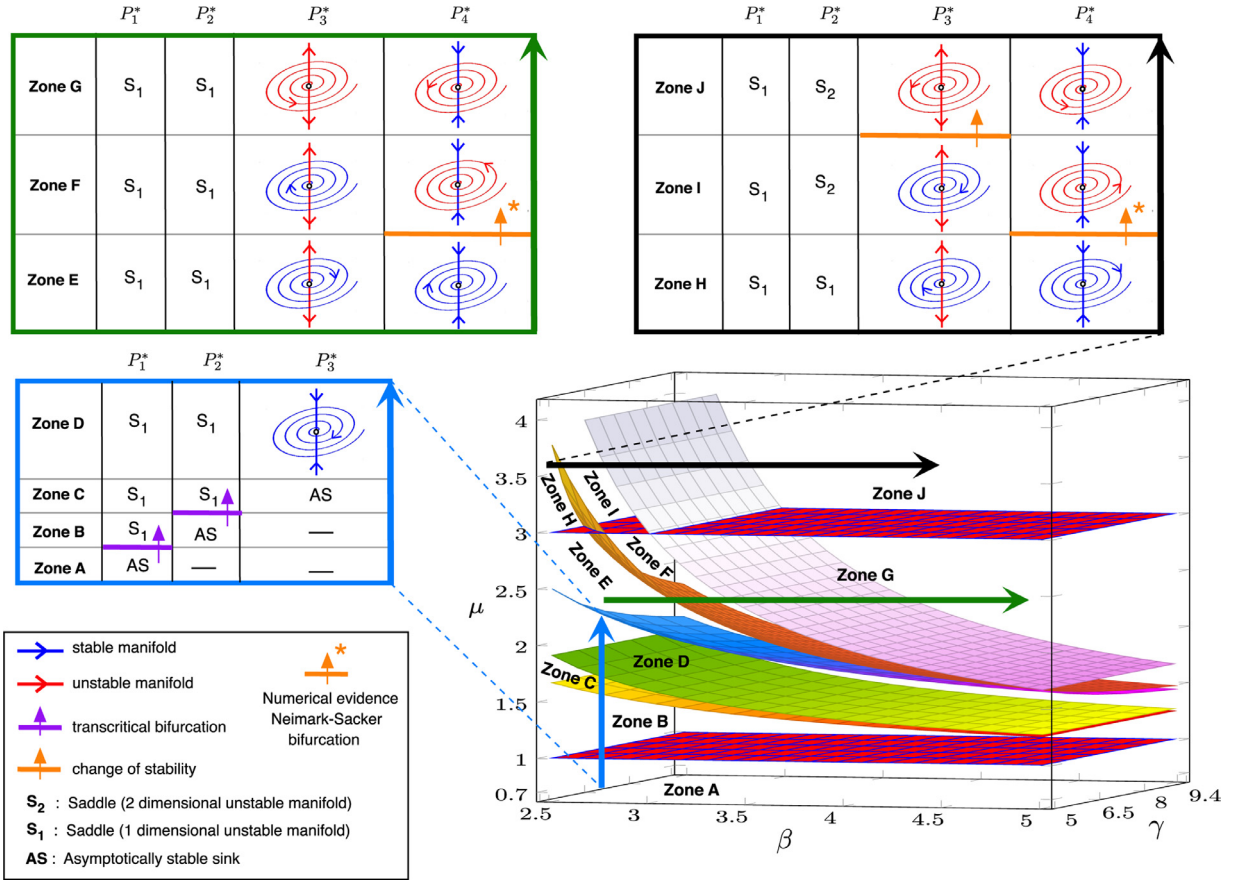

Fig. 7. Changes in the existence and local stability of the fixed points tied to the transitions between the zones identified in Fig. 6. The tables display, for each fixed point, the stability nature along the thick arrows displayed in the cuboid Q. The fixed points are classified as follows: asymptotically stable sink (AS); saddle with a 1-dimensional (S_1) and 2-dimensional (S_2) unstable invariant manifolds; and spirals (stable in blue; unstable in red), see the legend below the table framed in light blue. Stable and unstable manifolds are displayed with blue and red arrows, respectively. The small violet arrows in the lower table denote transcritical bifurcations, with collision of fixed points and stability changes. The small orange arrows indicate changes in stability. Here numerical evidences for supercritical Neimark-Sacker bifurcations have been obtained (indicated with an asterisk).

which has an eigenvalue $\lambda_{1,1} = \mu$ with eigenvector (1,0,0), and two eigenvalues $\lambda_{1,2} = \lambda_{1,3} = 0$ with eigenvectors (0,1,0) and (0,0,1) (see Fig. 6). Hereafter we will label the j−th eigenvalue of a fixed point P_i^* as $\lambda_{i,j}$, with $i = 1, \ldots, 4$ and $j = 1, \ldots, 3$. The assertion of the lemma follows from the Hartman-Grobman Theorem. □

Lemma 6. *The point $P_2^* = (1 - \mu^{-1}, 0, 0)$ is a boundary fixed point of the System (1) for all parameters such that $\mu \geq 1$. In particular, for all parameter values in* Q*, the fixed point P_2^* is non-hyperbolic if and only if:*

- $\mu = 1$, *that is, when* $P_2^* = P_1^*$;
- $\mu = \frac{\beta}{\beta - 1}$, *that is, when* $P_2^* = P_3^*$;
- $\mu = 3$.

The region of the parameter's cuboid where P_2^* is hyperbolic is divided into the following three layers:

$1 < \mu < \frac{\beta}{\beta-1}$: *$P_2^*$ is a locally asymptotically stable sink node that corresponds to the extinction of the two predator species.*
$\frac{\beta}{\beta-1} < \mu < 3$: *$P_2^*$ is a saddle with an unstable invariant manifold of dimension, 1 locally tangent to the x-axis.*
$3 < \mu \leq 4$: *P_2^* is a saddle with an unstable invariant manifold of dimension 2 locally tangent to the plane generated by the vectors (1,0,0) and* $(1, \frac{2-\mu}{\mu-1} - \frac{\beta}{\mu}, 0)$.

From Lemmas 5 and 6 it follows that when P_2^* bifurcates from P_1^* (exactly at $\mu = 1$), P_1^* changes its stability from attractor to saddle in a transcritical bifurcation.

Proof. The Jacobian matrix of System (1) at P_2^* is

$$J(P_2^*) = \begin{pmatrix} 2-\mu & 1-\mu & 1-\mu \\ 0 & \beta\left(1-\frac{1}{\mu}\right) & 0 \\ 0 & 0 & 0 \end{pmatrix},$$

which has:

- an eigenvalue $\lambda_{2,1} = 2-\mu$ with eigenvector (1,0,0),
- an eigenvalue $\lambda_{2,2} = \beta(1-\frac{1}{\mu})$ with eigenvector $(1, \frac{2-\mu}{\mu-1} - \frac{\beta}{\mu}, 0)$,
- and an eigenvalue $\lambda_{2,3} = 0$ with eigenvector $(1, 0, \frac{2-\mu}{\mu-1})$.

Moreover, for $1 \le \mu \le 4$ we have $2-\mu \in [-2, 1]$ and $\beta(1-\frac{1}{\mu}) \ge 0$. Clearly (see Fig. 6) one has:

- $2-\mu = \pm 1$ if and only if $\mu = 2 \mp 1$, and $|2-\mu| < 1$ if and only if $1 < \mu < 3$;
- $\beta(1-\frac{1}{\mu}) = 1$ if and only if $\mu = \frac{\beta}{\beta-1}$, and $0 \le \beta(1-\frac{1}{\mu}) < 1$ if and only if $1 \le \mu < \frac{\beta}{\beta-1}$;
- $1 < \frac{\beta}{\beta-1} < 3$ for every $\beta \in [2.5, 5]$.

Then the lemma follows from the Hartman-Grobman Theorem. □

Lemma 7. *The point $P_3^* = (\beta^{-1}, 1-\beta^{-1}-\mu^{-1}, 0)$ is a boundary fixed point of the System (1) for all positive parameters such that $\mu^{-1}+\beta^{-1} \le 1$. In particular, for all the parameters in* Q, *the fixed point P_3^* is non-hyperbolic if and only if:*

- $\mu = \frac{\beta}{\beta-1}$, *that is, when* $P_3^* = P_2^*$;
- $\mu = \frac{\beta\gamma}{(\beta-1)\gamma-\beta}$, *that is, when* $P_3^* = P_4^*$;
- $\mu = \frac{\beta}{\beta-2}$.

The region in Q *where P_3^* is hyperbolic is divided into the following four layers:*

$\frac{\beta}{\beta-1} < \mu \le 2\beta(\beta-1-\sqrt{\beta(\beta-2)})$: *$P_3^*$ is a locally asymptotically stable sink node. Here preys x and predators y achieve a static equilibrium.*

$2\beta(\beta-1-\sqrt{\beta(\beta-2)}) < \mu < \frac{\beta\gamma}{(\beta-1)\gamma-\beta}$: *$P_3^*$ is a locally asymptotically stable spiral-node sink. Here preys x and predators y achieve also a static equilibrium, reached via damped oscillations.*

$\frac{\beta\gamma}{(\beta-1)\gamma-\beta} < \mu < \min\{4, \frac{\beta}{\beta-2}\}$: *$P_3^*$ is an unstable spiral-sink node-source.*

$\min\{4, \frac{\beta}{\beta-2}\} < \mu \le 4$: *$P_3^*$ is an unstable spiral-node source.*

From Lemmas 6 and 7 it follows that when P_3^* bifurcates from P_2^* (at $\mu = \frac{\beta}{\beta-1}$),$P_2^*$ changes its stability from an attractor to a saddle again in a transcritical bifurcation.

Proof of Lemma 7. The Jacobian matrix of System (1) at P_3^* is

$$J(P_3^*) = \begin{pmatrix} 1-\frac{\mu}{\beta} & -\frac{\mu}{\beta} & -\frac{\mu}{\beta} \\ \beta\left(1-\frac{1}{\mu}\right)-1 & 1 & \beta\left(\frac{1}{\mu}-1\right)+1 \\ 0 & 0 & \gamma\left(1-\frac{1}{\beta}-\frac{1}{\mu}\right) \end{pmatrix},$$

and has eigenvalues

$$\lambda_{3,1} = \gamma\left(1-\tfrac{1}{\beta}-\tfrac{1}{\mu}\right), \text{ and}$$

$$\lambda_{3,2}, \lambda_{3,3} = 1-\frac{\mu}{2\beta} \pm \frac{\sqrt{\left(\beta+\frac{\mu}{2}\right)^2-\beta^2\mu}}{\beta}.$$

For $\frac{\beta}{\beta-1} \le \mu \le 4$ we have $\gamma(1-\frac{1}{\beta}-\frac{1}{\mu}) \ge 0$ and $\gamma(1-\frac{1}{\beta}-\frac{1}{\mu}) = 1$ if and only if $\mu = \frac{\beta\gamma}{(\beta-1)\gamma-\beta}$ (see Fig. 6). On the other hand, $(\beta+\frac{\mu}{2})^2-\beta^2\mu = 0$ if and only if $\mu = 2\beta(\beta-1\pm\sqrt{\beta(\beta-2)})$.

Now let us study the relation between $\frac{\beta}{\beta-1}, 2\beta(\beta-1\pm\sqrt{\beta(\beta-2)}), \frac{\beta\gamma}{(\beta-1)\gamma-\beta}$ and $\frac{\beta}{\beta-2}$. First we observe that, since $\beta \ge 2.5$,

$$2\beta\left(\beta-1+\sqrt{\beta(\beta-2)}\right) \ge 5(1.5+\sqrt{1.25}) > 13 > 4 \ge \mu.$$

Consequently, we simultaneously have $(\beta+\frac{\mu}{2})^2-\beta^2\mu = 0$ and $\mu \le 4$ if and only if $\mu = 2\beta(\beta-1-\sqrt{\beta(\beta-2)})$.

Second, since $\beta(\beta-2)=(\beta-1)^2-1$, it follows that

$$\beta(\beta-2)<(\beta-1)^2-1+\frac{1}{4(\beta-1)^2}=\left((\beta-1)-\tfrac{1}{2(\beta-1)}\right)^2.$$

Moreover, $\beta(\beta-2)>0$ and $(\beta-1)-\frac{1}{2(\beta-1)}>0$ (which follows from the inequality $2(\beta-1)^2>1$). So, the above inequality is equivalent to

$$\sqrt{\beta(\beta-2)}<(\beta-1)-\frac{1}{2(\beta-1)}\qquad\Longleftrightarrow\qquad\frac{1}{2(\beta-1)}<(\beta-1)-\sqrt{\beta(\beta-2)}$$

which, in turn, is equivalent to

$$\frac{\beta}{\beta-1}<2\beta\left(\beta-1-\sqrt{\beta(\beta-2)}\right).$$

Third, we will show that

$$2\beta\left(\beta-1-\sqrt{\beta(\beta-2)}\right)<\frac{\beta\gamma}{(\beta-1)\gamma-\beta}. \tag{3}$$

To this end observe that

$$\frac{\partial}{\partial\gamma}\frac{\gamma}{(\beta-1)\gamma-\beta}=-\frac{\beta}{((\beta-1)\gamma-\beta)^2}<0. \tag{4}$$

Hence, by replacing 9.4 by $\frac{47}{5}$,

$$\frac{47}{42\beta-47}=\frac{\frac{47}{5}}{\frac{47(\beta-1)}{5}-\beta}\le\frac{\gamma}{(\beta-1)\gamma-\beta}.$$

So, to prove (3), it is enough to show that

$$\beta-1-\sqrt{\beta(\beta-2)}<\frac{47}{2(42\beta-47)}\le\frac{1}{2\beta}\frac{\beta\gamma}{(\beta-1)\gamma-\beta}.$$

This inequality is equivalent to

$$\frac{84\beta^2-178\beta+47}{84\beta-94}=\beta-1-\frac{47}{84\beta-94}<\sqrt{\beta(\beta-2)}.$$

Since $\beta\ge 2.5$, $\frac{84\beta^2-178\beta+47}{84\beta-94}$ is positive and thus, it is enough to prove that

$$\frac{(84\beta^2-178\beta+47)^2}{(84\beta-94)^2}<\beta(\beta-2),$$

which is equivalent to

$$0<\beta(\beta-2)(84\beta-94)^2-(84\beta^2-178\beta+47)^2=840\beta^2-940\beta-2209.$$

This last polynomial is positive for every

$$\beta>\frac{47\sqrt{235}+235}{420}\approx 2.27499\cdots.$$

This ends the proof of (3). On the other hand, since $\gamma\ge 5\ge\beta$, we have $-\beta\gamma\le-\beta^2$ which is equivalent to

$$\beta\gamma(\beta-2)=\beta^2\gamma-2\beta\gamma\le\beta^2\gamma-\beta\gamma-\beta^2=\beta((\beta-1)\gamma-\beta),$$

and this last inequality is equivalent to

$$\frac{\beta\gamma}{(\beta-1)\gamma-\beta}\le\frac{\beta}{\beta-2}$$

(with equality only when $\gamma=5=\beta$). Thus, summarizing, we have seen:

$$1<\frac{\beta}{\beta-1}<2\beta\left(\beta-1-\sqrt{\beta(\beta-2)}\right)<\frac{\beta\gamma}{(\beta-1)\gamma-\beta}\le\frac{\beta}{\beta-2} \tag{5}$$

and the last inequality is an equality only when $\gamma=5=\beta$.

Next we study the modulus of the eigenvalues to determine the local stability of P_3^*. First observe (see Fig. 6) that $|\lambda_{3,1}|=|\gamma(1-\frac{1}{\beta}-\frac{1}{\mu})|<1$ if and only if $\frac{\beta}{\beta-1}<\mu<\frac{\beta\gamma}{(\beta-1)\gamma-\beta}$. On the other hand, on $\frac{\beta}{\beta-1}<\mu\le 2\beta(\beta-1-\sqrt{\beta(\beta-2)})$,

the discriminant $(\beta+\frac{\mu}{2})^2-\beta^2\mu$ is non-negative and the eigenvalues $\lambda_{3,2}$ and $\lambda_{3,3}$ are real. Moreover, $\beta>2$ is equivalent to $-\beta\mu>\beta\mu-\beta^2\mu$ and this to

$$\left(\beta-\tfrac{\mu}{2}\right)^2>\left(\beta+\tfrac{\mu}{2}\right)^2-\beta^2\mu \quad\Leftrightarrow\quad \beta-\frac{\mu}{2}>\sqrt{\left(\beta+\tfrac{\mu}{2}\right)^2-\beta^2\mu}$$

(observe that $\beta-\frac{\mu}{2}>0$ because $\beta>2$ and $\mu\le 4$, and recall that $\left(\beta+\frac{\mu}{2}\right)^2-\beta^2\mu$ is non-negative in the selected region). The last inequality above is equivalent to

$$1-\frac{\mu}{2\beta}>\frac{\sqrt{\left(\beta+\frac{\mu}{2}\right)^2-\beta^2\mu}}{\beta} \quad\Leftrightarrow\quad 0<1-\frac{\mu}{2\beta}-\frac{\sqrt{\left(\beta+\frac{\mu}{2}\right)^2-\beta^2\mu}}{\beta}=\lambda_{3,3}.$$

On the other hand, the following equivalent expressions hold:

$$\frac{\beta}{\beta-1}<\mu\Leftrightarrow\beta^2<\mu\beta(\beta-1)\Leftrightarrow\left(\beta+\tfrac{\mu}{2}\right)^2-\beta^2\mu=\beta^2+\frac{\mu^2}{4}+\mu\beta-\mu\beta^2<\frac{\mu^2}{4}$$

$$\frac{\sqrt{\left(\beta+\frac{\mu}{2}\right)^2-\beta^2\mu}}{\beta}<\frac{\mu}{2\beta}\Leftrightarrow\lambda_{3,2}=1-\frac{\mu}{2\beta}+\frac{\sqrt{\left(\beta+\frac{\mu}{2}\right)^2-\beta^2\mu}}{\beta}<1.$$

Summarizing, when $\frac{\beta}{\beta-1}<\mu\le 2\beta(\beta-1-\sqrt{\beta(\beta-2)})$ we have

$$0<\lambda_{3,3}=1-\frac{\mu}{2\beta}-\frac{\sqrt{\left(\beta+\frac{\mu}{2}\right)^2-\beta^2\mu}}{\beta}\le 1-\frac{\mu}{2\beta}+\frac{\sqrt{\left(\beta+\frac{\mu}{2}\right)^2-\beta^2\mu}}{\beta}=\lambda_{3,2}<1.$$

Consequently, P_3^* is a locally asymptotically stable sink node by (5), meaning that top predators (z) go to extinction and the other two species persist.

Now we consider the region $2\beta(\beta-1-\sqrt{\beta(\beta-2)})<\mu\le 4$. In this case the discriminant $(\beta+\frac{\mu}{2})^2-\beta^2\mu$ is negative and the eigenvalues $\lambda_{3,2}$ and $\lambda_{3,3}$ are complex conjugate with modulus

$$\sqrt{\left(1-\tfrac{\mu}{2\beta}\right)^2+\frac{\beta^2\mu-\left(\beta+\frac{\mu}{2}\right)^2}{\beta^2}}=\sqrt{\frac{\mu(\beta-2)}{\beta}}.$$

Clearly

$$\left|\sqrt{\frac{\mu(\beta-2)}{\beta}}\right|<1 \quad\Leftrightarrow\quad 2\beta\left(\beta-1-\sqrt{\beta(\beta-2)}\right)\le\mu\le\min\left\{4,\frac{\beta}{\beta-2}\right\}$$

(with equality only when $\gamma=5=\beta$). Then the lemma follows from the Hartman-Grobman Theorem. □

Lemma 8. *The point $P_4^*=(\rho,\gamma^{-1},\rho-\beta^{-1})$ with $\rho=\frac{1}{2}(1-\mu^{-1}+\beta^{-1}-\gamma^{-1})$ is a fixed point of the System (1) for all positive parameters satisfying that $\mu^{-1}+\beta^{-1}+\gamma^{-1}\le 1$. Moreover, for all the parameters in* Q*, there exists a function $\psi_4:[2.5,5]\times[5,9.4]\longrightarrow[\frac{\beta\gamma}{(\beta-1)\gamma-\beta},4)$ (whose graph Σ_4 is drawn in reddish colour in Fig. 6) such that P_4^* is non-hyperbolic if and only if:*

- $\mu=\frac{\beta\gamma}{(\beta-1)\gamma-\beta}$, *that is, when $P_4^*=P_3^*$;*
- $\mu=\psi_4(\beta,\gamma)$.

Furthermore, the region of the parameter's cuboid where P_4^* is hyperbolic is divided into the following two layers:

$\frac{\beta\gamma}{(\beta-1)\gamma-\beta}<\mu<\psi_4(\beta,\gamma)$: *$P_4^*$ is a locally asymptotically stable sink of spiral-node type. Within this first layer the three species achieve a static coexistence equilibrium with an oscillatory transient.*

$\psi_4(\beta,\gamma)<\mu\le 4$: *$P_4^*$ is an unstable spiral-source node-sink.*

Proof. The Jacobian matrix of System (1) at P_4^* is

$$J(P_4^*)=\begin{pmatrix}1-\mu\rho & -\mu\rho & -\mu\rho\\ \frac{\beta}{\gamma} & 1 & -\frac{\beta}{\gamma}\\ 0 & \gamma\left(\rho-\frac{1}{\beta}\right) & 1\end{pmatrix}.$$

The matrix $J(P_4^*)$ has eigenvalues

$$\lambda_{4,1} := 1 - \frac{\mu\rho}{3} + \frac{\sqrt[3]{\alpha}}{3\sqrt[3]{2}\sqrt{\gamma}} + \frac{\sqrt[3]{2}\big(\mu^2\rho^2\gamma - 3\beta(\mu+\gamma)\rho + 3\gamma\big)}{3\sqrt{\gamma}\sqrt[3]{\alpha}},$$

$$\lambda_{4,2}, \lambda_{4,3} := 1 - \frac{\mu\rho}{3} - \frac{\sqrt[3]{\alpha}}{3\sqrt[3]{16}\sqrt{\gamma}}(1 \mp \sqrt{3}i) - \frac{\mu^2\rho^2\gamma - 3\beta(\mu+\gamma)\rho + 3\gamma}{3\sqrt[3]{4}\sqrt{\gamma}\sqrt[3]{\alpha}}\big(1 \pm \sqrt{3}i\big),$$

where

$$\begin{aligned}
\alpha = \ & -2\gamma^{3/2}\rho^3\mu^3 - 45\gamma^{3/2}\beta\mu\rho^2 + 9\mu^2\rho^2\beta\sqrt{\gamma} + 45\gamma^{3/2}\rho\mu + \sqrt{27\widetilde{\alpha}}, \text{ and} \\
\widetilde{\alpha} := \ & 8(\rho\beta - 1)\left(\mu^4\rho^4 + \frac{71(\rho\beta-1)\rho^2\mu^2}{8} + \frac{(\beta\rho-1)^2}{2}\right)\gamma^3 \\
& - 38(\rho\beta - 1)\left(\mu^2\rho^2 - \frac{6(\rho\beta-1)}{19}\right)\rho\beta\mu\gamma^2 \\
& - \mu^2\rho^2\beta^2\big(\mu^2\rho^2 - 12(\rho\beta-1)\big)\gamma + 4\beta^3\mu^3\rho^3.
\end{aligned}$$

When $\mu = \frac{\beta\gamma}{(\beta-1)\gamma-\beta}$ we clearly have

$$J(P_4^*) = \begin{pmatrix} 1-\mu\rho & -\mu\rho & -\mu\rho \\ \frac{\beta}{\gamma} & 1 & -\frac{\beta}{\gamma} \\ 0 & 0 & 1 \end{pmatrix}$$

and

$$\begin{pmatrix} 1-\mu\rho & -\mu\rho & -\mu\rho \\ \frac{\beta}{\gamma} & 1 & -\frac{\beta}{\gamma} \\ 0 & 0 & 1 \end{pmatrix}\begin{pmatrix} 1 \\ -2 \\ 1 \end{pmatrix} = \begin{pmatrix} 1 \\ -2 \\ 1 \end{pmatrix}.$$

Thus, for every $(\beta,\ \gamma) \in [2.5,\ 5] \times [5,\ 9.4]$, $\lambda_{4,1} = 1$ when $\mu = \frac{\beta\gamma}{(\beta-1)\gamma-\beta}$. Moreover, it can be seen numerically that for every $(\beta,\ \gamma) \in [2.5,\ 5] \times [5,\ 9.4]$, $\lambda_{4,1}$ is a strictly decreasing function of μ such that $\lambda_{4,1} > -1$ when $\mu = 4$. So, $\lambda_{4,1}$ only breaks the hyperbolicity of P_4^* in the surface $\mu = \frac{\beta\gamma}{(\beta-1)\gamma-\beta}$ and $|\lambda_{4,1}| < 1$ in the region

$$(\beta, \gamma, \mu) \in [2.5, 5] \times [5, 9.4] \times \left(\tfrac{\beta\gamma}{(\beta-1)\gamma-\beta}, 4\right].$$

Next we need to describe the behaviour of $|\lambda_{4,2}| = |\lambda_{4,3}|$ as a function of μ. The following statements have been observed numerically:

(i) $|\lambda_{4,2}| = |\lambda_{4,3}| < 1$ for every

$$(\beta, \gamma, \mu) \in [2.5, 5] \times [5, 9.4] \times \left\{\tfrac{\beta\gamma}{(\beta-1)\gamma-\beta}\right\} \setminus \left\{\left(5, 5, \tfrac{\beta\gamma}{(\beta-1)\gamma-\beta}\right)\right\}$$

and $|\lambda_{4,2}| = |\lambda_{4,3}| = 1$ at the point $(\beta, \gamma, \mu) = (5, 5, \frac{\beta\gamma}{(\beta-1)\gamma-\beta})$.

(ii) $|\lambda_{4,2}| = |\lambda_{4,3}| > 1$ for every $(\beta,\ \gamma,\ \mu) \in [2.5,\ 5] \times [5,\ 9.4] \times \{4\}$.

(iii.1) There exists a Non-Monotonic (NM) region denoted NM_4 which is contained in the rectangle $[2.5,\ 2.59597\cdots] \times [5,\ 6.49712\cdots]$ such that for every $(\beta, \gamma) \in \mathsf{NM}_4$ there exists a value $\mu^*(\beta, \gamma) \in (\frac{\beta\gamma}{(\beta-1)\gamma-\beta}, 4)$ with the property that $|\lambda_{4,2}| = |\lambda_{4,3}|$ is a strictly decreasing function of the parameter $\mu \in [\frac{\beta\gamma}{(\beta-1)\gamma-\beta}, \mu^*(\beta, \gamma)]$, and a strictly increasing function of μ for every value of $\mu \in [\mu^*(\beta,\ \gamma),\ 4]$. In particular, from (i) it follows that $|\lambda_{4,2}| = |\lambda_{4,3}| < 1$ holds for every point $(\beta, \gamma, \mu) \in \mathsf{NM}_4 \times [\frac{\beta\gamma}{(\beta-1)\gamma-\beta}, \mu^*(\beta, \gamma)]$.
Consequently, for every $(\beta, \gamma) \in \mathsf{NM}_4$, there exists a unique value of the parameter $\mu = \psi_4(\beta, \gamma) > \mu^*(\beta, \gamma)$ such that $|\lambda_{4,2}| = |\lambda_{4,3}| = 1$ at the point $(\beta,\ \gamma,\ \psi_4(\beta,\ \gamma))$.

The region NM_4, as shown in the picture at the side, is delimited by the axes $\beta = 2.5$, $\gamma = 5$ and, approximately, by the curve $\gamma \approx 19.6981\beta^2 - 115.98\beta + 173.334$.

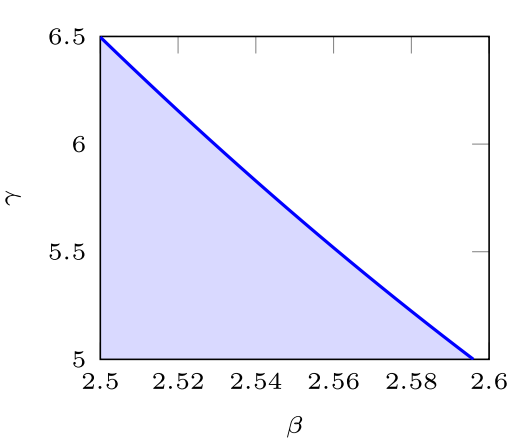

(iii.2) For every $(\beta, \gamma) \in ([2.5, 5] \times [5, 9.4]) \setminus \mathsf{NM}_4, |\lambda_{4,2}| = |\lambda_{4,3}|$ is a strictly increasing function of μ. In particular, from (i) it follows that there exists a unique value of $\mu = \psi_4(\beta, \gamma) > \frac{\beta\gamma}{(\beta-1)\gamma-\beta}$ such that $|\lambda_{4,2}| = |\lambda_{4,3}| = 1$ at the point $(\beta, \gamma, \psi_4(\beta, \gamma))$.

Then the lemma follows from the Hartman-Grobman Theorem. □

4. Local bifurcations: three dimensional bifurcation diagram

Due to the mathematical structure of the Map (1) and to the number of parameters one can provide analytical information on local dynamics within different regions of the chosen parameter space. That is, to build a three-dimensional bifurcation diagram displaying the parametric regions involved in the local dynamics of the fixed points investigated above. These analyses also provide some clues on the expected global dynamics, addressed in Sections 5 and 6. To understand the local dynamical picture, the next lemma relates all the surfaces that play a role in defining the local structural stability zones in the previous four lemmas. It justifies the relative positions of these surfaces, shown in Fig. 6.

We define

$$\mathsf{H}_4 := \{(\beta, \gamma) : \psi_4(\beta, \gamma) \geq 3\}.$$

Lemma 9. *The relations between the surfaces defined in Lemmas 5–8 are the following:*

(i) *For every* $(\beta, \gamma) \in [2.5, 5] \times [5, 9.4]$,

$$1 < \frac{\beta}{\beta-1} < 2\beta\left(\beta - 1 - \sqrt{\beta(\beta-2)}\right) < \frac{\beta\gamma}{(\beta-1)\gamma-\beta}.$$

H_4 *is the region contained in* $[2.5, 2.769\cdots] \times [5, 6.068\cdots]$ *and delimited by the axes* $\beta = 2.5$ *and* $\gamma = 5$, *and the curve* $\gamma \approx 2.13725\beta^2 - 15.2038\beta + 30.7162$.

(ii) *For every* $(\beta, \gamma) \in ([2.5, \frac{8}{3}] \times [5, 9.4]) \cap \mathsf{H}_4$,

$$\frac{\beta\gamma}{(\beta-1)\gamma-\beta} < 3 \leq \psi_4(\beta, \gamma) < 4 \leq \frac{\beta}{\beta-2}.$$

On the other hand, for every $(\beta, \gamma) \in ([2.5, \frac{8}{3}] \times [5, 9.4]) \setminus \mathsf{H}_4$,

$$\frac{\beta\gamma}{(\beta-1)\gamma-\beta} < \psi_4(\beta, \gamma) < 3 < 4 \leq \frac{\beta}{\beta-2}.$$

(iii) *For every* $(\beta, \gamma) \in ((\frac{8}{3}, 3) \times [5, 9.4]) \cap \mathsf{H}_4$,

$$\frac{\beta\gamma}{(\beta-1)\gamma-\beta} < 3 \leq \psi_4(\beta, \gamma) < \frac{\beta}{\beta-2} < 4$$

For every $(\beta, \gamma) \in ((\frac{8}{3}, 3) \times [5, 9.4]) \setminus \mathsf{H}_4$,

$$\frac{\beta\gamma}{(\beta-1)\gamma-\beta} < \psi_4(\beta, \gamma) < 3 < \frac{\beta}{\beta-2} < 4.$$

(iv) *For every* $(\beta, \gamma) \in \{3\} \times [5, 9.4]$,

$$\frac{\beta\gamma}{(\beta-1)\gamma-\beta} < \psi_4(\beta,\gamma) < 3 = \frac{\beta}{\beta-2}.$$

(v) *For every* $(\beta, \gamma) \in (3, 5] \times [5, 9.4]$,

$$\frac{\beta\gamma}{(\beta-1)\gamma-\beta} \le \psi_4(\beta,\gamma) \le \frac{\beta}{\beta-2} < 3.$$

Moreover, all the above inequalities are strict except in the point $(\beta, \gamma) = (5, 5)$ *where* $\frac{\beta\gamma}{(\beta-1)\gamma-\beta} = \psi_4(\beta,\gamma) = \frac{\beta}{\beta-2}$.

Proof. Statement (i) follows from Eq. (5) and the fact that H_4 is the region delimited by the axes $\beta = 2.5$ and $\gamma = 5$, and the curve

$$\gamma \approx 2.13725\beta^2 - 15.2038\beta + 30.7162$$

can be checked numerically.

On the other hand, observe that for every $\gamma \in [5, 9.4]$ we have

$$\begin{cases} \frac{\beta}{\beta-2} \ge 4 & \text{for } \beta \in \left[2.5, \frac{8}{3}\right], \\ 4 > \frac{\beta}{\beta-2} > 3 & \text{for } \beta \in \left(\frac{8}{3}, 3\right), \\ \frac{\beta}{\beta-2} = 3 & \text{for } \beta = \frac{8}{3}, \\ 3 > \frac{\beta}{\beta-2} & \text{for } \beta \in (3, 5]. \end{cases}$$

Moreover, $7\beta > 15$ is equivalent to $12\beta - 15 > 5\beta$, and Eq. (4) implies

$$3 > \frac{5\beta}{4\beta-5} = \beta\frac{5}{5(\beta-1)-\beta} \ge \beta\frac{\gamma}{(\beta-1)\gamma-\beta}.$$

So, Statements (ii–v) follow from these observations, from Eq. (5) and by checking numerically the various relations of $\psi_4(\beta, \gamma)$ with $\mu = \frac{\beta\gamma}{(\beta-1)\gamma-\beta}$, $\mu = 3$, and $\mu = \frac{\beta}{\beta-2}$ for the different regions considered in Statements (ii–v). □

The detailed description of the local dynamics in the zones of Fig. 6 (see also Fig. 7) is given by the following (see Lemmas 5–9):

Theorem 10. *The following statements hold:*

Zone A: $(\beta, \gamma, \mu) \in [2.5, 5] \times [5, 9.4] \times (0, 1)$.
In this layer the system has $P_1^* = (0, 0, 0)$ *as a unique fixed point. This fixed point is a locally asymptotically stable sink node, meaning that the three species go to extinction. Indeed, it is proved in Theorem 11 that this is a globally asymptotically stable (GAS) point.*

Zone B: $(\beta, \gamma, \mu) \in [2.5, 5] \times [5, 9.4] \times (1, \frac{\beta}{\beta-1})$.
In this zone the system has exactly two fixed points: the origin P_1^* *and* $P_2^* = (1 - \frac{1}{\mu}, 0, 0)$. P_1^* *is a saddle (*$\dim W^u(P_1^*) = 1$*) with an invariant manifold locally tangent to the x-axis.* P_2^* *is a locally asymptotically stable sink node. Hence, in this zone only preys will survive. Theorem 15 proves that in this zone* P_2^* *is a GAS point.*

Zone C: $(\beta, \gamma, \mu) \in [2.5, 5] \times [5, 9.4] \times (\frac{\beta}{\beta-1}, 2\beta(\beta - 1 - \sqrt{\beta(\beta-2)}))$.
In this region the system has exactly three fixed points: the origin P_1^*, P_2^* *and* $P_3^* = (\beta^{-1}, 1 - \beta^{-1} - \mu^{-1}, 0)$. P_1^* *and* P_2^* *are saddles with* $\dim W^u(P_1^*, P_2^*) = 1$ *and* P_3^* *is a locally asymptotically stable sink node. Here top predators can not survive, being the system only composed of preys and the predator species y.*

Zone D: $(\beta, \gamma, \mu) \in [2.5, 5] \times [5, 9.4] \times (2\beta(\beta - 1 - \sqrt{\beta(\beta-2)}), \frac{\beta\gamma}{(\beta-1)\gamma-\beta})$.
In this zone the system still has three fixed points: P_1^*, P_2^* *and* P_3^*. P_1^* *and* P_2^* *are saddles with* $\dim W^u(P_1^*, P_2^*) = 1$ *but* P_3^* *is a locally asymptotically stable spiral-node sink. In this region the prey and predator y reach a static equilibrium of coexistence achieved via damped oscillations, while the top predator z goes to extinction.*

Zone E: $(\beta, \gamma, \mu) \in [2.5, 5] \times [5, 9.4] \times (\frac{\beta\gamma}{(\beta-1)\gamma-\beta}, \min\{3, \psi_4(\beta,\gamma)\})$.
In this layer the system has exactly four fixed points: the origin P_1^*, P_2^*, P_3^* *and* $P_4^* = (\rho, \gamma^{-1}, \rho - \beta^{-1})$. P_1^* *and* P_2^* *are saddle points with* $\dim W^u(P_1^*, P_2^*) = 1$, *the fixed point* P_3^* *is an unstable spiral-sink node-source and* P_4^* *is a locally asymptotically stable sink of spiral-node type. Under this scenario, the three species achieve a static coexistence state also via damped oscillations.*

Zone F: $(\beta, \gamma, \mu) \in (([2.5, 5] \times [5, 9.4]) \setminus \mathsf{H}_4) \times (\psi_4(\beta,\gamma), \min\{3, \frac{\beta}{\beta-2}\})$.
In this layer the system has exactly four fixed points: the origin P_1^*, P_2^*, P_3^* *and* $P_4^* = (\rho, \gamma^{-1}, \rho - \beta^{-1})$. *The fixed points* P_1^* *and* P_2^* *are saddles with* $\dim W^u(P_1^*, P_2^*) = 1$, *the point* P_3^* *is an unstable spiral-sink node-source and* P_4^* *is an unstable spiral-source node-sink. Here, due to the unstable nature of all fixed points, fluctuating coexistence of all of the species is found. As we will see in Section 6, this coexistence can be governed by periodic or chaotic fluctuations.*

Zone G: $(\beta,\gamma,\mu)\in(3,5]\times[5,9.4]\times(\frac{\beta}{\beta-2},3)$.
In this zone the system has four fixed points: P_1^*, P_2^*, P_3^* and P_4^*.P_1^* and P_2^* are a saddles with $\dim W^u(P_1^*,P_2^*)=1$, P_3^* is an unstable spiral-node source and P_4^* is an unstable spiral-source node-sink. The expected coexistence dynamics here are like those of zone F above.

Zone H: $(\beta,\gamma,\mu)\in \mathsf{H}_4\times(3,\psi_4(\beta,\gamma))$.
In this region the system has four fixed points: P_1^*, P_2^*, P_3^* and P_4^*. The fixed points P_1^* and P_2^* are saddles $\dim W^u(P_1^*,P_2^*)=1$,P_3^* is an unstable spiral-sink node-source and P_4^* is a locally asymptotically stable sink of spiral-node type. The dynamics here are the same as the ones in zone E.

Zone I: $(\beta,\gamma,\mu)\in(2.5,3)\times[5,9.4]\times(\max\{3,\psi_4(\beta,\gamma)\},\min\{4,\frac{\beta}{\beta-2}\})$.
In this zone the system has four fixed points: P_1^*, P_2^*, P_3^* and P_4^*.P_1^* is a saddle with $\dim W^u(P_1^*)=1$, P_2^* is a saddle with $\dim W^u(P_2^*)=2$, P_3^* is an unstable spiral-sink node-source and P_4^* is an unstable spiral-source node-sink. Here the dynamics can be also governed by coexistence among the three species via oscillations.

Zone J: $(\beta,\gamma,\mu)\in(\frac{8}{3},5]\times[5,9.4]\times(\max\{3,\frac{\beta}{\beta-2}\},4)$.
In this zone the system has four fixed points: P_1^*, P_2^*, P_3^* and P_4^*. The fixed point P_1^* is a saddle with $\dim W^u(P_1^*)=1$, the point P_2^* is a saddle with $\dim W^u(P_2^*)=2$, P_3^* is an unstable spiral-node source and P_4^* is an unstable spiral-source node-sink. Dynamics here can also be governed by all-species fluctuations, either periodic or chaotic.

Fig. 7 provides a summary of the changes in the existence and local stability of the fixed points for each one of the zones identified. Also, we provide an animation of the dynamical outcomes tied to crossing the cuboid following the direction of the dashed thick blue arrow represented in Fig. 6. Specifically, Movie-3.mp4 displays the dynamics along this line for variable x_n, as well as in the phase space (x, y) and (x, y, z).

5. Some remarks on global dynamics

In this section we study the global dynamics in Zones A and B from the preceding section.

Theorem 11 (Global dynamics in Zone A)**.** *Assume that $\mu<1$ and let (x, y, z) be a point from $\mathcal{S}$. Then,*

$$\lim_{n\to\infty} T^n(x,y,z)=(0,0,0)=P_1^*.$$

In what follows, $\lambda_\mu(\sigma):=\mu\sigma(1-\sigma)$ will denote the logistic map.

Proof of Theorem 11. From Fig. 6 (or Lemmata 5–8) it follows that (0,0,0) is the only fixed point of T whenever $\mu<1$ and it is locally asymptotically stable.

We denote $(x_0,y_0,z_0)=(x,y,z)\in\mathcal{S}$ and $(x_n,y_n,z_n)=T^n(x,y,z)\in\mathcal{S}\subset\mathcal{E}$ for every $n\geq 1$. Assume that there exists $n\geq 0$ such that $y_n=0$. Then, substituting $(x_n, 0, z_n)$ into Eq. (1) it follows that $y_{n+1}=z_{n+1}=0$ and so

$$T^{n+1}(x,y,z)=(x_{n+1},0,0)\in[0,1]\times\{0\}\times\{0\},$$

and $T^{n+1+k}(x,y,z)=(\lambda_\mu^k(x_{n+1}),0,0)$ for every $k\geq 0$. Since, $\mu<1$, one gets $\lim_{k\to\infty}\lambda_\mu^k(\sigma)=0$ for every $\sigma\in[0,1]$. So, the proposition holds in this case.

In the rest of the proof we assume that $y_n>0$ for every $n\geq 0$. We claim that

$$x_n\leq\frac{\mu^n}{4}$$

for every $n\geq 1$. Let us prove the claim. Since $(x,y,z)\in\mathcal{S}\subset\mathcal{E}$ (Proposition 2) with $y>0$ we have $x\geq z\geq 0$ and $x+y+z\leq 1$. Thus,

$$x_1=\mu x(1-x-y-z)\leq\mu x(1-x)\leq\frac{\mu}{4},$$

which proves the case $n=1$. Assume now that the claim holds for some $n\geq 1$ and prove it for $n+1$. As before, $(x_n,y_n,z_n)\in\mathcal{E}$ with $y_n>0$ implies $x_n\geq z_n\geq 0$ and $x_n+y_n+z_n\leq 1$. Hence,

$$x_{n+1}=\mu x_n(1-x_n-y_n-z_n)\leq\mu x_n\leq\mu\frac{\mu^n}{4}=\frac{\mu^{n+1}}{4}.$$

On the other hand, by using again the assumption that $(x_n,y_n,z_n)\in\mathcal{E}$ with $1\geq y_n>0$ for every $n\geq 0$, and the definition of T in (1), we get that $x_n>z_n\geq 0$ for every $n\geq 0$. Moreover, $y_{n+1}=\beta y_n(x_n-z_n)\leq\beta y_n x_n\leq\beta x_n$. Hence, for every $n\geq 0$,

$$0\leq z_n<x_n\leq\frac{\mu^n}{4}\quad\text{and}\quad 0<y_n\leq\beta x_{n-1}\leq\beta\frac{\mu^{n-1}}{4}.$$

This implies that $\lim_{n\to\infty}(x_n,y_n,z_n)=(0,0,0)$ because $\mu<1$. □

To study the global dynamics in Zone B we need three simple lemmas. The first one is on the logistic map; the second one relates the first coordinate of the image of T with the logistic map; the third one is technical.

Lemma 12 (On the logistic map). *Let $1 < \mu < 2$ and set $I_0 := [\alpha_\mu, \widetilde{\alpha}_\mu]$ where $0 < \alpha_\mu = 1 - \frac{1}{\mu} < \frac{1}{2}$ is the stable fixed point of λ_μ and $\frac{1}{2} < \widetilde{\alpha}_\mu < 1$ is the unique point such that $\lambda_\mu(\widetilde{\alpha}_\mu) = \alpha_\mu$. Set also $I_{n+1} := \lambda_\mu(I_n) \subset I_n$ for every $n \geq 0$. Then, for every $\varepsilon > 0$ there exists $N \geq 1$ such that $I_N \subset [\alpha_\mu, \alpha_\mu + \varepsilon)$.*

Proof. The fact that $0 < \alpha_\mu = 1 - \frac{1}{\mu} < \frac{1}{2}$ is a stable fixed point of λ_μ for $1 < \mu < 2$ is well known. Also, since $\lambda_\mu|_{[\alpha_\mu, \frac{1}{2}]}$ is increasing and $1 < \mu < 2$, it follows that

$$\alpha_\mu = \lambda_\mu\left(\alpha_\mu\right) < \ldots < \lambda_\mu^{n+1}\left(\tfrac{1}{2}\right) < \lambda_\mu^{n}\left(\tfrac{1}{2}\right) < \ldots < \lambda_\mu^{2}\left(\tfrac{1}{2}\right) < \lambda_\mu\left(\tfrac{1}{2}\right) < \tfrac{1}{2}.$$

Therefore,

$$I_1 = \lambda_\mu\left(I_0\right) = \lambda_\mu\left(\left[\alpha_\mu, \tfrac{1}{2}\right]\right) = \left[\alpha_\mu, \lambda_\mu\left(\tfrac{1}{2}\right)\right] \subset \left[\alpha_\mu, \tfrac{1}{2}\right] \subset I_0$$

and, for every $n \geq 1$, one gets

$$I_{n+1} = \lambda_\mu\left(I_n\right) = \left[\alpha_\mu, \lambda_\mu^{n+1}\left(\tfrac{1}{2}\right)\right] \subsetneq \left[\alpha_\mu, \lambda_\mu^{n}\left(\tfrac{1}{2}\right)\right] = I_n \subset \left[\alpha_\mu, \tfrac{1}{2}\right].$$

Then, the lemma follows from the fact that $\lim_{n\to\infty} \lambda_\mu^n\left(\frac{1}{2}\right) = \alpha_\mu$. □

Lemma 13. *Let $(x_0, y_0, z_0) \in \mathcal{S}$ and set*

$$(x_n, y_n, z_n) = T(x_{n-1}, y_{n-1}, z_{n-1}) \in \mathcal{E}$$

for every $n \geq 1$. Then, for every $n \geq 1$,

$$0 \leq x_n = \lambda_\mu(x_{n-1}) - \mu x_{n-1}(y_{n-1} + z_{n-1}) \leq \lambda_\mu(x_{n-1})$$

and, when $\mu \leq 2$, it follows that $0 \leq x_n \leq \lambda_\mu^n(x_0) \leq \frac{1}{2}$.

Proof. The first statement can be proved as follows:

$$\begin{aligned} x_n &= \mu x_{n-1}(1 - x_{n-1}) - \mu x_{n-1}(y_{n-1} + z_{n-1}) \\ &= \lambda_\mu(x_{n-1}) - \mu x_{n-1}(y_{n-1} + z_{n-1}) \leq \lambda_\mu(x_{n-1}) \end{aligned}$$

(notice that $\mu, x_n, x_{n-1}, y_{n-1}, z_{n-1} \geq 0$ because $(x_n, y_n, z_n) \in \mathcal{E}$ for every n).

The second statement for $n = 1$ follows directly from the first statement and from the fact that $\lambda_\mu([0, 1]) = \lambda_\mu([0, \frac{1}{2}]) \subset [0, \frac{1}{2}]$ whenever $\mu \leq 2$.

Assume now that the second statement holds for some $n \geq 1$. Then, from the first statement of the lemma and the fact that $\mu \leq 2$ we have

$$0 \leq x_{n+1} \leq \lambda_\mu(x_n) \leq \lambda_\mu\left(\lambda_\mu^n(x_0)\right) = \lambda_\mu^{n+1}(x_0) \leq \lambda_\mu\left(\tfrac{1}{2}\right) \leq \tfrac{1}{2},$$

because $\lambda_\mu|_{[0, \frac{1}{2}]}$ is increasing. □

The proof of the next technical lemma is straightforward.

Lemma 14 (The damped logistic map). *Let $\lambda_{\mu,s}(\sigma) := s\lambda_\mu(\sigma) = \mu s\sigma(1 - \sigma)$ denote the damped logistic map defined on the interval [0,1]. Assume that $1 < \mu < 2$ and $\frac{1}{\mu} < s < 1$. Then the following properties of the damped logistic map hold:*

(a) $\lambda_{\mu,s}(\sigma) < \lambda_\mu(\sigma)$ *for every* $0 < \sigma < 1$.

(b) $\lambda_{\mu,s}(0) = 0$ *and* $\lambda_{\mu,s}\Big|_{\left[0, \frac{1}{2}\right]}$ *is strictly increasing.*

(c) $\lambda_{\mu,s}$ *has exactly one stable fixed point* $\alpha_{\mu,s} := 1 - \frac{1}{\mu s}$ *with derivative*

$$\lambda'_{\mu,s}(\alpha_{\mu,s}) = \lambda'_{\mu,s}(\sigma)\big|_{\sigma=\alpha_{\mu,s}} = \mu s(1 - 2\sigma)\big|_{\sigma=\alpha_{\mu,s}} = 2 - \mu s < 1\,.$$

(d) *For every* $\sigma \in (0, \alpha_{\mu,s})$ *we have*

$$\sigma < \lambda_{\mu,s}(\sigma) < \lambda_{\mu,s}^2(\sigma) < \ldots < \alpha_{\mu,s}$$

and $\lim_{k\to\infty} \lambda_{\mu,s}^k(\sigma) = \alpha_{\mu,s}$.

Theorem 15 (Global dynamics in Zone B). *Assume that $1 < \mu < \frac{\beta}{\beta - 1}$ and let (x, y, z) be a point from $\mathcal{S}$. Then, either $T^n(x, y, z) = (0, 0, 0)$ for some $n \geq 0$ or*

$$\lim_{n\to\infty} T^n(x, y, z) = \left(1 - \mu^{-1}, 0, 0\right) = P_2^*.$$

Remark 16. From Lemma 4 it follows that the unique fixed points which exist in this case are P_1^* and P_2^*.

Proof. From Fig. 6 (or Lemmata 5–14) it follows that $(\alpha_\mu, 0, 0)$ with $\alpha_\mu := 1 - \frac{1}{\mu}$ is the only locally asymptotically stable fixed point of T. In the whole proof we will consider that α_μ is the unique stable fixed point of λ_μ. As in previous proofs, we denote $(x_0, y_0, z_0) = (x, y, z) \in \mathcal{S}$ and $(x_n, y_n, z_n) = T^n(x, y, z) \in \mathcal{E}$ for every $n \geq 1$.

If there exists $n \geq 0$ such that $(x_n, y_n, z_n) = (0, 0, 0)$ we are done. Thus, in the rest of the proof we assume that $(x_n, y_n, z_n) \neq (0, 0, 0)$ for every $n \geq 0$.

Assume that there exists $n \geq 0$ such that $y_n = 0$. By the definition of T, it follows that $T^{n+1}(x, y, z) = (x_{n+1}, 0, 0) \in [0, 1] \times \{0\} \times \{0\}$, and, consequently, $T^{n+1+k}(x, y, z) = (\lambda_\mu^k(x_{n+1}), 0, 0)$ for every $k \geq 0$. Thus, since

$$1 < \mu < \tfrac{\beta}{\beta-1} \leq \tfrac{5}{3} < 2,$$

it turns out that $\lim_{k\to\infty} \lambda_\mu^k(x_{n+1}) = \alpha_\mu$ (recall that we are in the case $(x_n, y_n, z_n) \neq (0, 0, 0)$ for every $n \geq 0$ and, consequently, $\lambda_\mu^k(x_{n+1}) \neq 0$ for every $k \geq 0$). So, the proposition holds in this case.

In the rest of the proof we are left with the case $(x_n, y_n, z_n) \in \mathcal{E}$ and $y_n > 0$ for every $n \geq 0$. Moreover, suppose that $x_n = 0$ for some $n \geq 0$. Since $(x_n, y_n, z_n) \in \mathcal{E}$ we have that $0 \leq z_n \leq x_n = 0$ implies $z_n = 0$. Consequently, $(x_{n+1}, y_{n+1}, z_{n+1}) = T(x_n, y_n, z_n) = (0, 0, 0)$, a contradiction. Thus, $x_n, y_n > 0$ for every $n \geq 0$.

Observe that, since $\mu < \frac{\beta}{\beta-1}$ we have

$$\alpha_\mu = \frac{\mu-1}{\mu} < \left.\frac{\mu-1}{\mu}\right|_{\mu=\frac{\beta}{\beta-1}} = \tfrac{1}{\beta}.$$

On the other hand, $\lambda'_\mu(\alpha_\mu) = \mu(1-2x)|_{x=\frac{\mu-1}{\mu}} = 2-\mu < 1$ because $\mu > 1$. Thus, there exist $r \in (2-\mu, 1)$ and $0 < \delta < \alpha_\mu$ such that $\alpha_\mu + \delta < \frac{1}{\beta} \leq \frac{2}{5} < \frac{1}{2}$, and $\lambda'_\mu(x) < r$ for every $x \in (\alpha_\mu - \delta, \alpha_\mu + \delta)$.

Set $\tau := \beta(\alpha_\mu + \delta) < 1$. To show that $\lim_{n\to\infty}(x_n, y_n, z_n) = (\alpha_\mu, 0, 0)$ we will prove that the following two statements hold:

(i) There exists a positive integer N such that

$$0 \leq y_n < \tau^{n-N} \quad \text{and} \quad 0 \leq z_n < \gamma\tau^{n-1-N},$$

for every $n \geq N+2$.

(ii) For every $0 < \varepsilon < \delta$ there exists a positive integer M such that $\left|x_n - \alpha_\mu\right| < \varepsilon$ for all $n \geq M$.

To prove (i) and (ii) we fix $0 < \varepsilon < \delta < \alpha_\mu$ and we claim that there exists a positive integer $N = N(\varepsilon)$ such that $x_n < \alpha_\mu + \varepsilon$ for every $n \geq N$. Now we prove the claim. Assume first that $x_0 \in \left[0, \alpha_\mu\right] \cup \left[\widetilde{\alpha}_\mu, 1\right]$, where $\frac{1}{2} < \widetilde{\alpha}_\mu < 1$ is the unique point such that $\lambda_\mu\left(\widetilde{\alpha}_\mu\right) = \alpha_\mu$. Since

$$\lambda_\mu\left(\left[0, \alpha_\mu\right] \cup \left[\widetilde{\alpha}_\mu, 1\right]\right) = \lambda_\mu\left(\left[0, \alpha_\mu\right]\right) = \left[0, \alpha_\mu\right],$$

$\lambda_\mu^n(x_0) \in \left[0, \alpha_\mu\right]$ for every $n \geq 1$. Thus, if we set $N = N(\varepsilon) = 1$ and we take $n \geq N$, by Lemma 13 we have

$$0 \leq x_n \leq \lambda_\mu^n(x_0) \leq \alpha_\mu < \alpha_\mu + \varepsilon.$$

Assume now that $x_0 \in \left(\alpha_\mu, \widetilde{\alpha}_\mu\right)$. By Lemmas 13 and 12, there exists $N = N(\varepsilon) \geq 1$ such that

$$0 \leq x_n \leq \lambda_\mu^n(x_0) \in I_n \subset I_N \subset \left[\alpha_\mu, \alpha_\mu + \varepsilon\right)$$

for every $n \geq N$. This ends the proof of the claim.

Now we prove (i). From the above claim we have

$$\beta x_n < \beta\left(\alpha_\mu + \varepsilon\right) < \beta\left(\alpha_\mu + \delta\right) = \tau < 1 \quad \text{for every } n \geq N. \tag{6}$$

Consequently, by the iterative use of (6), for every $n \geq N+2$ we have

$$\begin{aligned} y_n = \beta y_{n-1}(x_{n-1} - z_{n-1}) \leq \beta y_{n-1} x_{n-1} < \tau y_{n-1} < \\ \tau^2 y_{n-2} < \cdots < \tau^{n-N} y_N \leq \tau^{n-N}, \end{aligned}$$

and $z_n = \gamma y_{n-1} z_{n-1} \leq \gamma y_{n-1} < \gamma\tau^{n-1-N}$.

Now we prove (ii). In this proof we will use the damped logistic map $\lambda_{\mu,s}$ with parameter $1 > s > \frac{1}{\mu\varepsilon+1}$. From (i) it follows that there exists a positive integer $\widetilde{M} \geq N+2$ such that

$$y_n + z_n < \min\left\{\frac{\beta(1-r)}{\mu\tau}\varepsilon, (1-s)\left(1 - (\alpha_\mu - \varepsilon)\right)\right\}$$

for every $n \geq \widetilde{M}$. Observe that if there exists $M \geq \widetilde{M}$ such that $|x_M - \alpha_\mu| < \varepsilon$, then $|x_n - \alpha_\mu| < \varepsilon$ for every $n \geq M$. To prove it assume that there exists $n \geq M$ such that $|x_k - \alpha_\mu| < \varepsilon$ for $k = M, M+1, \ldots, n$ and prove it for $n+1$. By Lemma 13, Eq. (6) and the Mean Value Theorem,

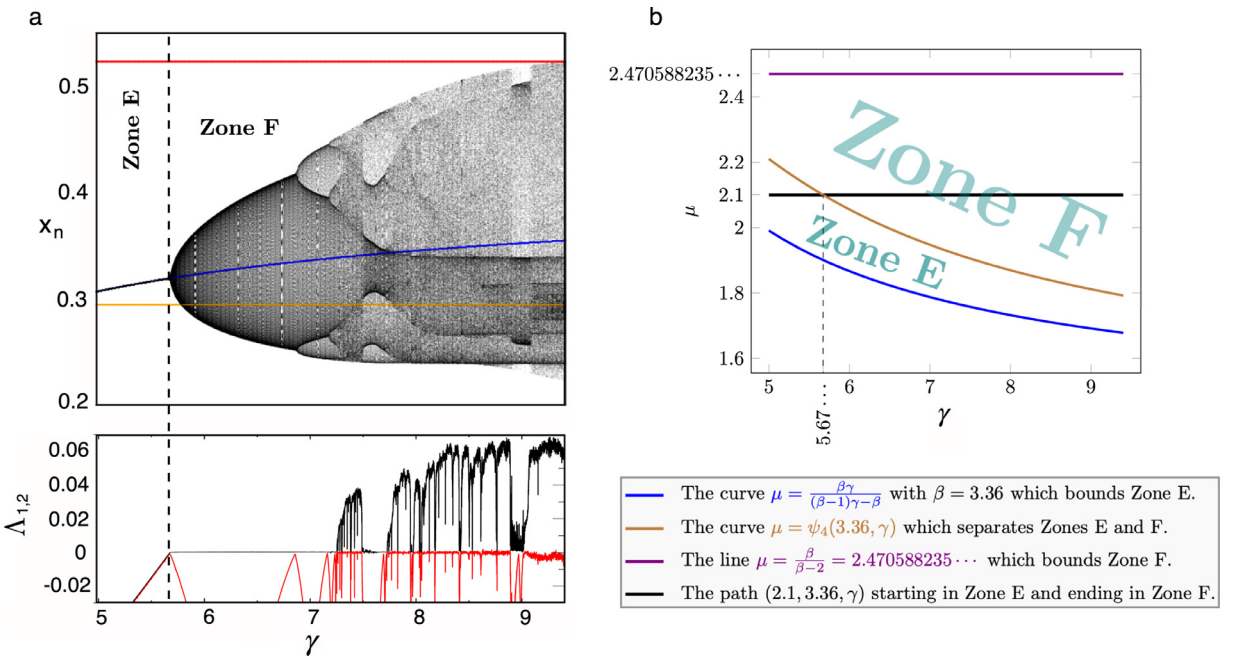

Fig. 8. (a, upper) Bifurcation diagram displaying the dynamics of preys x when increasing the predation intensity of predator z on predator y, given by γ, using $\mu = 2.1$ and $\beta = 3.36$. This range of γ covers zones E and F, separated by the vertical dashed line. The values of the fixed points are shown overlapped, with P_2^*: red; P_3^*: orange; and P_4^*: blue. (a, lower) Spectrum of Lyapunov exponents, $\Lambda_{1,2,3}$ computed for the same range of γ used in the bifurcation diagram (for clarity only $\Lambda_{1,2}$ are displayed, in black and red respectively). In both panels the initial conditions are: $x_0 = 0.1$, $y_0 = 0.02$, and $z_0 = 0.03$. (b) A cut of the parameter space at $\beta = 3.36$ showing the path $(\mu = 2.1, \beta = 3.36, \gamma)$ followed by the bifurcation diagram of (a). The dynamics for this parameter range can be visualised in Movie-4.mp4.

$$\begin{aligned}|x_{n+1} - \alpha_\mu| &= \left|\lambda_\mu(x_n) - \alpha_\mu - \mu x_n(y_n + z_n)\right| \\ &\le \left|\lambda_\mu(x_n) - \lambda_\mu(\alpha_\mu)\right| + \mu x_n(y_n + z_n) \\ &= \lambda'_\mu(\xi)|x_n - \alpha_\mu| + \mu x_n(y_n + z_n) \\ &< \lambda'_\mu(\xi)\varepsilon + \mu\frac{\tau}{\beta}\frac{\beta(1-r)}{\mu\tau}\varepsilon = \varepsilon\left(\lambda'_\mu(\xi) + (1-r)\right),\end{aligned}$$

where ξ is a point between x_n and α_μ. Since $|\xi - \alpha_\mu| \le |x_n - \alpha_\mu| < \varepsilon < \delta$ it follows that $\lambda'_\mu(\xi) < r$. So, $|x_{n+1} - \alpha_\mu| < \varepsilon(\lambda'_\mu(\xi) + (1-r)) < \varepsilon$.

To end the proof of the proposition we have to show that there exists $M \ge \widetilde{M}$ such that $|x_M - \alpha_\mu| < \varepsilon$. By the above claim we know that $x_{\widetilde{M}} < \alpha_\mu + \varepsilon$. So, the statement holds trivially with $M = \widetilde{M}$ whenever $x_{\widetilde{M}} > \alpha_\mu - \varepsilon$.

In the rest of the proof we may assume that $0 < x_{\widetilde{M}} \le \alpha_\mu - \varepsilon$. Observe that $\varepsilon < \delta < \alpha_\mu = \frac{\mu-1}{\mu}$ implies $\mu\varepsilon < \mu - 1$, which is equivalent to $\mu\varepsilon + 1 < \mu$ and, consequently, $\frac{1}{\mu} < \frac{1}{\mu\varepsilon+1} < s < 1$. So, s verifies the assumptions of Lemma 14. Moreover, since $\frac{1}{\mu\varepsilon+1} < s$, we have

$$1 < s(\mu\varepsilon + 1) \iff \mu s - 1 > \mu s - \mu s\varepsilon - s \iff \mu(\mu s - 1) > \mu s\left(\mu(1-\varepsilon) - 1\right),$$

which is equivalent to $\alpha_{\mu,s} = \frac{\mu s - 1}{\mu s} > \frac{\mu(1-\varepsilon)-1}{\mu} = \alpha_\mu - \varepsilon$. Summarising, we have, $0 < x_{\widetilde{M}} \le \alpha_\mu - \varepsilon < \alpha_{\mu,s}$.

By Lemma 14(d), there exists $L > 0$ such that $\lambda^L_{\mu,s}(x_{\widetilde{M}}) > \alpha_\mu - \varepsilon$. If there exists $N < \widetilde{M} < M < \widetilde{M} + L$ such that $x_M > \alpha_\mu - \varepsilon$ then, $|x_M - \alpha_\mu| < \varepsilon$ because, by the above claim, $x_M < \alpha_\mu + \varepsilon$. Hence, we may assume that $x_{\widetilde{M}+k} \le \alpha_\mu - \varepsilon$ for every $k = 0, 1, \ldots, L-1$. Then,

$$\mu x_{\widetilde{M}}\left(y_{\widetilde{M}} + z_{\widetilde{M}}\right) < \mu x_{\widetilde{M}}(1-s)\left(1 - (\alpha_\mu - \varepsilon)\right) \le (1-s)\mu x_{\widetilde{M}}\left(1 - x_{\widetilde{M}}\right) = (1-s)\lambda_\mu\left(x_{\widetilde{M}}\right),$$

which, by Lemmas 13 and 14(b), is equivalent to

$$0 < \lambda_{\mu,s}\left(x_{\widetilde{M}}\right) = s\lambda_\mu\left(x_{\widetilde{M}}\right) < \lambda_\mu\left(x_{\widetilde{M}}\right) - \mu x_{\widetilde{M}}\left(y_{\widetilde{M}} + z_{\widetilde{M}}\right) = x_{\widetilde{M}+1}\,.$$

Moreover, by iterating these computations and using again Lemma 14(b) we have

$$0 < \lambda^2_{\mu,s}\left(x_{\widetilde{M}}\right) < \lambda_{\mu,s}\left(x_{\widetilde{M}+1}\right) < x_{\widetilde{M}+2}$$

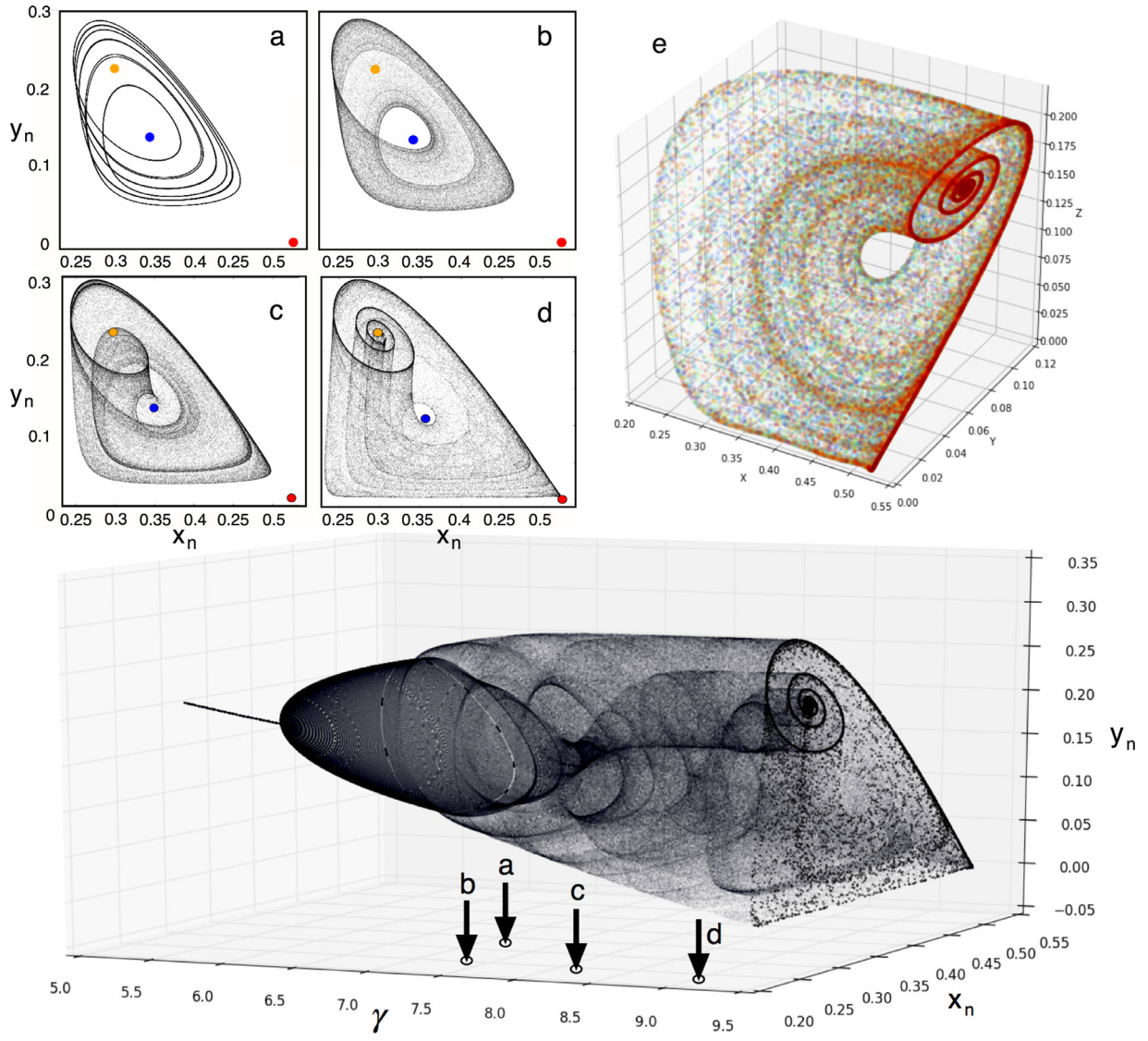

Fig. 9. Three-dimensional bifurcation diagram plotting the population values (x, y) using the predator rate of predator z as control parameter, setting $\mu = 2.1$ and $\beta = 3.36$. The attractors above the bifurcation diagram are displayed using: (a) $\gamma = 7.3$; (b) $\gamma = 7.46$; (c) $\gamma = 8.14$, and (d) $\gamma = 9.14$. All of the attractors are in zone *F*. The fixed points are shown in the phase space, with P_2^*: red; P_3^*: orange; and P_4^*: blue. The initial conditions are the same than in Fig. 8. In (e) we display the full chaotic attractor using $\gamma = 9.14$ (note that the full attractor is a discrete Shilnikov-like connection). Here the color gradient corresponds to time: red dots are longer times. See also Movie-4.mp4.

(notice that $x_{\tilde{M}+1} < \frac{1}{2}$ by Lemma 13). Thus, by repeating the process we get $0 < \lambda_{\mu,s}^k(x_{\tilde{M}}) < x_{\tilde{M}+k}$ for every $k = 0, 1, \ldots, L$. This implies that

$$\alpha_\mu - \varepsilon < \lambda_{\mu,s}^L\left(x_{\tilde{M}}\right) < x_{\tilde{M}+L},$$

and the statement holds with $M = \tilde{M} + L$. □

6. Chaos and Lyapunov exponents

As expected, iteration of Map (1) suggests the presence of chaotic attractors (see Fig. 9(c-e) and Fig. 10(e,f)). In order to identify chaos we compute Lyapunov exponents, labelled Λ_i, using the computational method described in [44, pages 74–80], which provides the full spectrum of Lyapunov exponents for the Map (1).

Let us explore the dynamics of the system focusing on the strength of predation, parametrised by constants γ and β. To do so we first investigate the dynamics increasing the predation rate of predator z on predator y, given by γ. We have built a bifurcation diagram displaying the dynamics of the prey species x by iterating Eq. (1) when increasing γ,

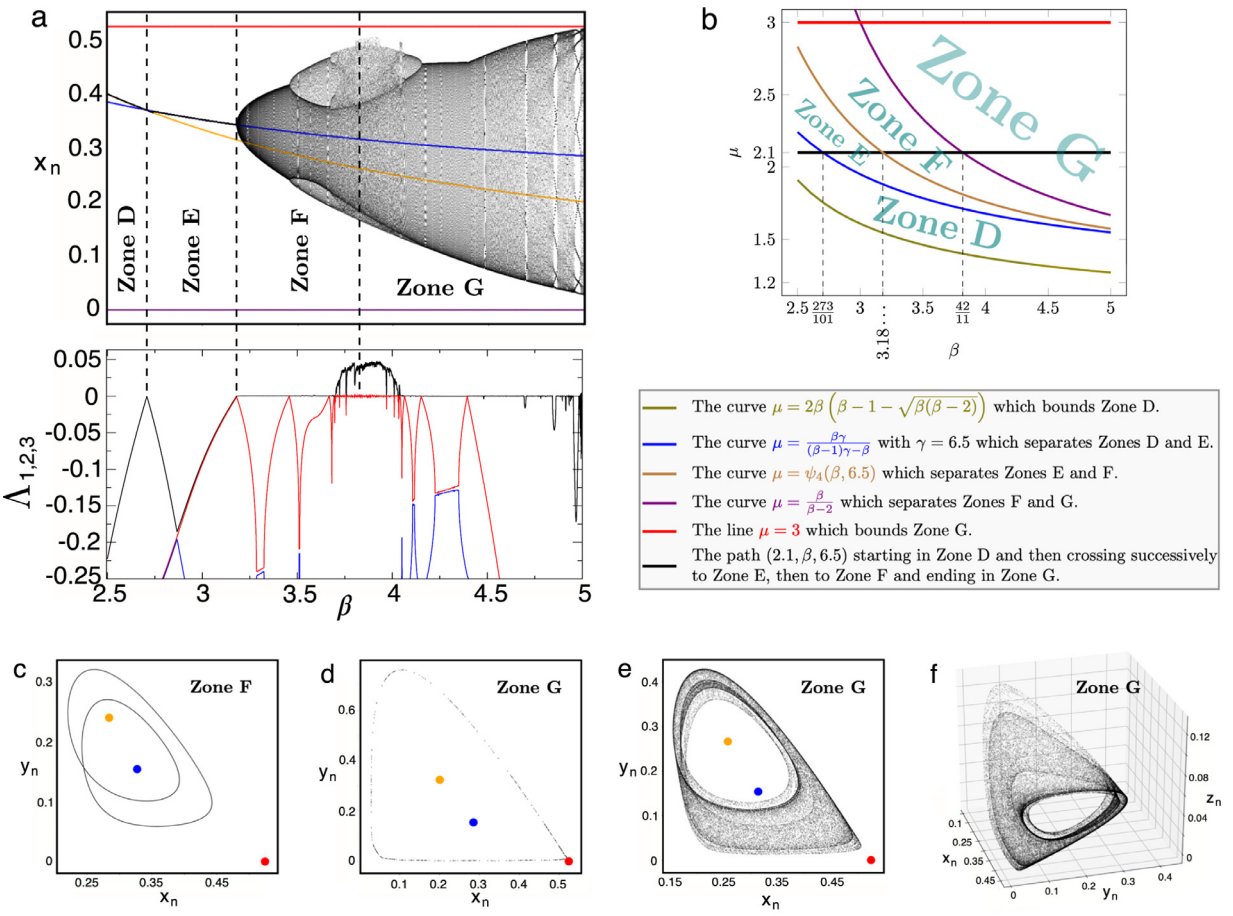

Fig. 10. (a) Bifurcation diagram displaying preys' dynamics when increasing the rate of predation of predator y (constant β) on the prey x. The explored range of β goes from zones D to G (changes between zones are indicated with vertical dashed lines). Here the values of the fixed points when increasing β are also displayed (P_2^*: red; P_3^*: orange; and P_4^*: blue). Below we plot the spectrum of Lyapunov exponents, Λ_i, for the same range of β. Here we fix $\mu = 2.1$ and $\gamma = 6.5$. The initial conditions are the same than in the previous figure. (b) A cut of the parameter space at $\gamma = 6.5$ showing the path (2.1, β, 6.5). Three projected attractors are shown with: (c) $\beta = 3.52$ (zone F); (d) $\beta = 4.99$ and (e, f) $\beta = 3.89$ (zone G). The dynamics tied to the increase of β can be visualised in Movie-5.mp4.

setting $\mu = 2.1$ and $\beta = 3.36$ (see Fig. 8(a)). The increase in γ for these fixed values of μ and β makes the dynamics to change between zones $E \to F$ (see also Fig. 8(b)). For $5 < \gamma < 5.673555\cdots$, populations achieve a static coexistence equilibrium at P_4^*, which is achieved via damped oscillations (see the properties in zone E). Increasing γ involves the entry into zone F, where all of the fixed points have an unstable nature and thus periodic and chaotic solutions are found. Here we find numerical evidences of a route to chaos driven by period-doubling of invariant closed curves that appears after a supercritical Neimark-Sacker (Hopf-Andronov) bifurcation for maps (flows) [45,46]. This bifurcation happens when the maximal Lyapunov exponent is zero (see the range $5.673555 < \gamma \lesssim 7.25$) and the eigenvalues at the fixed point P_4^* (which is locally unstable) are complex. Notice that the first Neimark-Sacker bifurcation marks the change from zones E to F (indicated with a vertical dashed line in Fig. 8). This means that an increase in the predation rate of species z unstabilises the dynamics and the three species fluctuate chaotically. Fig. 9 displays the same bifurcation diagram than in Fig. 8, represented in the three-dimensional space (γ, x, y), where it can be shown how the attractors change by increasing γ. Here we also display several projections of periodic (Fig. 9(a)) and chaotic (Fig. 9(b-d)) attractors. Fig. 9(e) displays the full chaotic attractor. For an animated visualisation of the dynamics dependence on γ we refer the reader to Movie-4.mp4.

To further investigate the dynamics considering another key ecological parameter, we study the dynamics increasing the predation strength of predator y on preys x, which is given by parameter β. As an example we have selected the range $2.5 \leq \beta \leq 5$, which corresponds to one of the sides of Q. Here the range of β follows the next order of crossing of the zones in Q when increasing β: $D \to E \to F \to G$.Fig. 10(a) shows the bifurcation diagram also obtained by iteration. In Fig. 10(b) we also provide a diagram of the stability zones crossed in the bifurcation diagram. Here, for $2.5 \leq \beta < 273/101$ the dynamics falls into zone D, for which the top predator z goes to extinction and the prey and predator y achieve a static equilibrium. Increasing β involves the entry into zone E (exactly at $\beta = 273/101$), the region where the fixed point of all-species coexistence is asymptotically locally stable. Counter-intuitively, stronger predation of y on x makes the three species

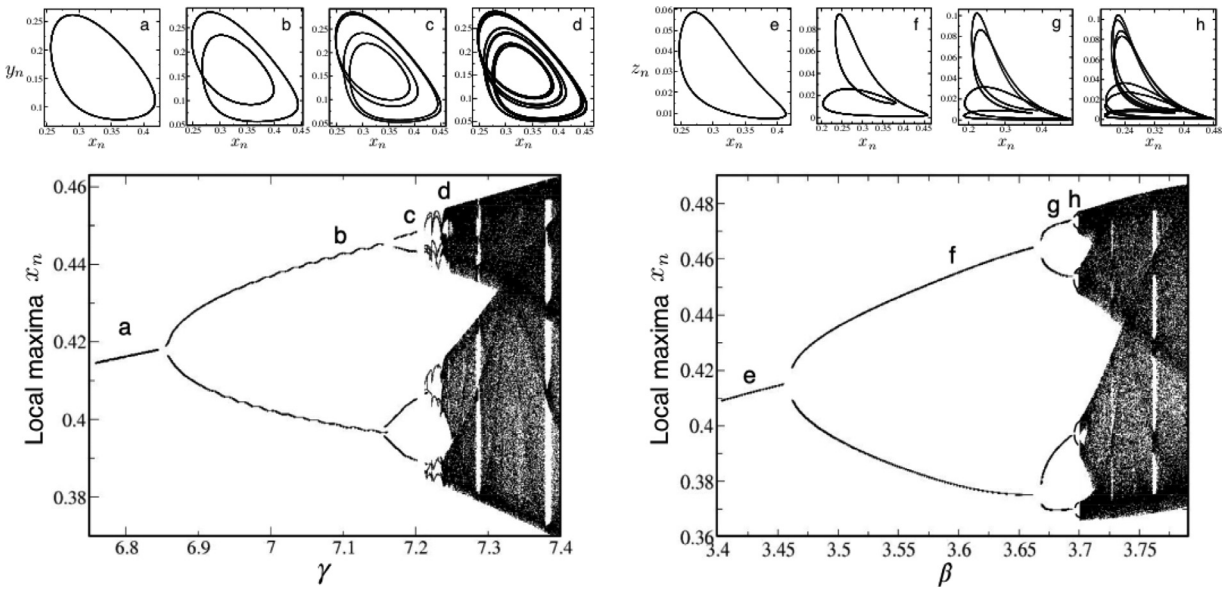

Fig. 11. Route to chaos when increasing predation rates governed by period-doubling of invariant curves. We display the local maxima of time series x_n on the attractor for γ (left diagram with $\beta = 3.36$) and β (diagram at the right with $\gamma = 6.5$). Above the diagrams we display the attractors projected on the phase planes (x, y) and (x, z), with: (a) $\gamma = 6.8$, (b) $\gamma = 7.1$, (c) $\gamma = 7.18$, (d) $\gamma = 7.21$, (e) $\beta = 3.425$, (f) $\beta = 3.6$, (g) $\beta = 3.685$, and (h) $\beta = 3.7$. In all the plots the initial conditions are $x_0 = 0.2, y_0 = 0.02, z_0 = 0.03$. See Movie-6.mp4 for a visualisation of the full attractor and the time series x_n, y_n, and z_n undergoing period-doubling of closed curves tied to the bifurcations diagram at the left, shown within the range $6.75 \leq \gamma \leq 8$.

to coexist, avoiding the extinction of the top predator z. At $\beta \approx 3.1804935$ there is another change to zone F, where all of the fixed points are unstable and thus periodic dynamics can occur. As we previously discussed, this is due to a series of bifurcations giving place to chaos. We notice that further increase of β involves another change of zone. Precisely, at $\beta = 42/11 = 3.\overline{81}$ the system changes from zone F to G. Several attractors are displayed in Fig. 10: a period-two invariant curve (panel c) with $\beta = 3.52$ and $\Lambda_1 = 0$ projected onto the phase space (x, y), found in zone F; and two attractors in zone G, given by a chaotic attractor with $\beta = 4.99$ and $\Lambda_1 = 0.0044\cdots$ (panel (d) in Fig. 10); and another chaotic attractor found at $\beta = 3.89$ (here $\Lambda_1 = 0.047\cdots$), shown in a projection (panel e) and in the full phase space (panel f). Movie-5.mp4 displays the dynamics tied to the bifurcation diagram shown in Fig. 10.

6.1. Route to chaos: period-doublings of invariant curves

It is known that some dynamical systems can enter into a chaotic regime by means of different and well-defined routes [45]. The most familiar ones are: (i) the period-doubling route (also named Feigenbaum scenario); (ii) the Ruelle-Takens-Newhouse route; (iii) and the intermittency route (also named Manneville-Pomeau route). The Feigenbaum scenario is the one identified in the logistic equation for maps, which involves a cascade of period doublings of fixed points that ultimately end up in chaos [7]. The Ruelle-Takens-Newhouse involves the appearance of invariant curves that change to tori and then by means of tori bifurcations become unstable and strange chaotic attractors appear. Finally, the intermittency route, tied to fold bifurcations, involves a progressive appearance of chaotic transients which increase in length as the control parameter is changed, finally resulting in a strange chaotic attractor.

The bifurcation diagrams computed in Figs. 8 and 10 seem to indicate that after a Neimark-Sacker bifurcation, the new invariant curves undergo period-doublings (see e.g., the beginning from Zone F until the presence of chaos in Fig. 10(a)). In order to characterise the routes to chaos at increasing the predation parameters γ and β, we have built bifurcation diagrams by plotting the local maxima of time series for x_n for each value of these two parameters. The time series have been chosen after discarding a transient of $3 \cdot 10^4$ iterations to ensure that the dynamics is in the attractor. The plot of the local maxima allows to identify the number of maxima of the invariant curves as well as of the attractors, resulting in one maximum for a period-1 invariant curve, two maxima for period-2 curves, etc. In the chaotic region the number of maxima appears to be extremely large (actually infinite). The resulting bifurcation diagram thus resembles the celebrated period-doubling scenario of periodic points (Feigenbaum scenario). We must notice that previous works have found period doublings of tori towards chaotic transitions [47–49].

The results are displayed in Fig. 11 by using γ and β as bifurcation parameters. We note that the bifurcation diagram for γ, despite clearly showing the branches after the first period-doubling, presented a noisy aspect. This could be due to a sampling of the local maxima on the invariant curve not being perfectly closed. That is, the invariant curve for the selected parameter values seems to be much more hyperbolic (i.e., attracting) for the diagram computed with β in Fig. 11, since this

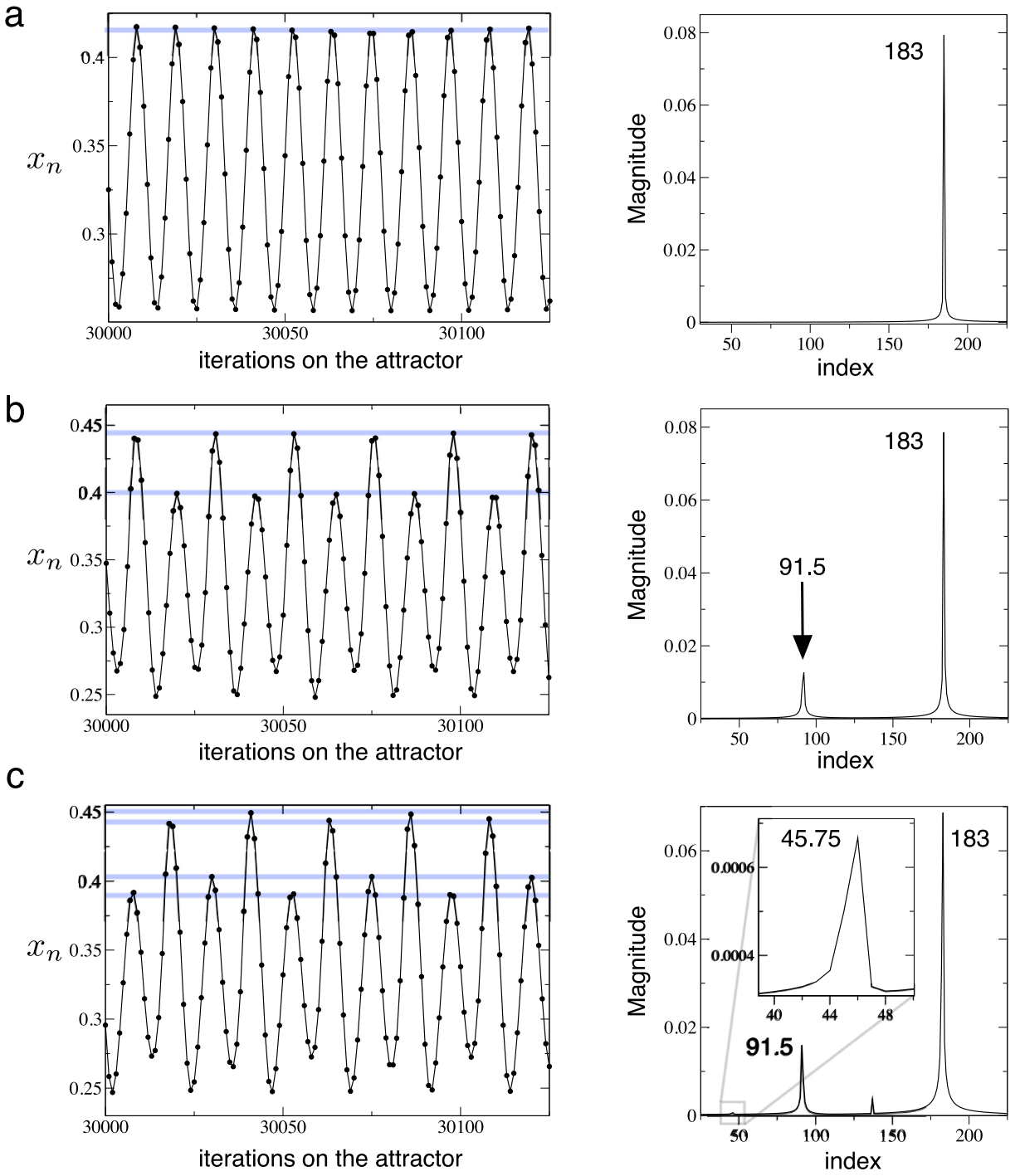

Fig. 12. Period-doublings of invariant curves represented with the time series of the prey x for the values of γ: (a) $\gamma = 6.8$, (b) $\gamma = 7.1$, and (c) $\gamma = 7.18$ (the same values of the left picture in Fig. 11). For better visualisation we have overlapped blue horizontal lines indicating the maxima of the time series. Note that in (c) the highest periods appear to be very close (see also the attractor (c) in the previous figure). The fast Fourier transforms for these three curves seem to show numerical evidence of a period doubling phenomenon. The FFT analysis of time series (c) contains an enlarged view of the peak at index 45.75, which is half the one found at 91.5 and a quarter of 183, all of them providing the most relevant coefficients (their modulus, in fact) of their DFT and, therefore, the main frequency of each discrete curve.

noisy effect was not observed at all. To smooth this effect we have used running averages, which, despite showing these small waves, produced a better bifurcation diagram. For both γ and β, it seems clear that the invariant curves undergo period doublings. We also have plotted the resulting attractors for period-1,2,4,8 orbits (see e.g. Fig. 11(a–d) for the case with γ using projections on the (x, y) space).

We have finally performed a Fast Fourier Transform (FFT) of the time series for x_n on the attractor corresponding to the attractors displayed in Fig. 11(a–d) and Fig. 11(e–h). The FFT emphasises the main frequencies (or periods) composing the signal by showing the modulus of their Fourier coefficients. Remember that FFT provides an efficient and fast way to compute the Discrete Fourier Transform, DFT in short, of a discrete signal: given $x_0, x_1, \ldots, x_{N-1}$ complex numbers, its DFT is defined as the sequence $f_0, f_1, \ldots, f_{N-1}$ determined by

$$f_j = \sum_{k=0}^{N-1} x_k \exp\left(\frac{-2\pi \mathrm{i} jk}{N}\right).$$

The FFTs have been computed using times series of 2^{11} points after discarding the first $3 \cdot 10^4$ iterations of the map (a transitory). The results are displayed in Fig. 12 for the dynamics displayed in panels (a-d) of Fig. 11. Similar results have been obtained for the dynamics in panels (e-h) of Fig. 11 (results not shown). These FFTs have been performed using a rectangular data window, and we have plotted the index of the signal versus its magnitude. It can be observed, by direct inspection, that the first relevant coefficient (in fact, its modulus) appear at each graph at half the index of the previous one (upper). This can be a numerical evidence of a period doubling (see also the animation in Movie-6.mp4 to visualise the changes in the time series and in the attractor at increasing γ). Here the period doubling of the curves can be clearly seen. A deeper study on the characterisation of this period-doubling scenario will be carried out in future work by computing the linking and rotation numbers of the curves.

7. Conclusions

The investigation of ecological dynamical systems has been of wide interest as a way to understand the dynamical complexity of ecosystems, which are inherently nonlinear. Such nonlinearities arise from density-dependent processes typically given by intra- or inter-specific competition between species, by cooperative interactions, or by antagonistic processes such as prey-predator or host-parasite dynamics. Three-species food chain systems have been widely investigated, especially for time-continuous systems [11,32–36]. Key aspects of the complexity of the dynamics such as topological entropy measures [32] as well as of different chaos-generating mechanisms [32–36] have been discussed for these systems, which considered in many cases functional responses for predators and different time scales i.e., slower dynamics at the higher trophic levels [33–36]. Discrete models have been also widely used to model the population dynamics of species with non-overlapping generations [6,7,9]. Indeed, several experimental research on insect dynamics revealed a good matching between the observed dynamics and the ones predicted by discrete dynamical models such as maps [4,5,22,23].

Typically, discrete models can display irregular or chaotic dynamics even when one or two species are considered [6,7,37–39]. Additionally, the study of the local and global dynamics for multi-species discrete models is usually performed numerically (by iterating the associated map) and most of the times fixing the rest of the parameters to certain values. Hence, a full analysis within a given region of the parameter space is often difficult due to the dimension of the dynamical system and to the number of model parameters. In this article we extend a previous two-dimensional map describing predator-prey dynamics [40]. The extension consists in including a top predator to a predator-prey model, resulting in a three species food chain. This new model considers that the top predator consumes the predators that in turn consume preys. Also, the top predator interacts negatively with the growth of the prey e.g., due to predation or competition. Finally, the prey also undergoes intra-specific competition.

We here provide a detailed analysis of local and global dynamics of the model within a given volume of the full parameter space containing relevant dynamics. The so-called *escaping set*, causing sudden populations extinctions, is identified. These escaping sets contain zones in which the iterates go out of the domain of the invariant set (e.g., surpassing the carrying capacity), then making population densities to become negative (these scenarios are here considered as extinctions, albeit the discrete nature of time). For some parameter values these escaping regions appear to have a complex, fractal structure.

Several parametric zones are identified, for which different dynamical outcomes exist: all-species extinctions, extinction of the top predator, extinction of both predators, and persistence of the three species in different coexistence attractors. Periodic and chaotic regimes are identified by means of numerical bifurcation diagrams and of Lyapunov exponents. We have identified a period-doubling route of invariant curves to chaos tuning the predation rates of both predators. This route involves a supercritical Neimark-Sacker bifurcation giving rise to a closed invariant curve responsible of all-species coexistence. Despite this route to chaos has been found for parameters which tune predation rates, future work should address how robust is this route to chaos for other parameter combinations of Map (1). Interestingly, we find that this route to chaos for the case of increasing predation directly on preys (tuning β) can involve an unstable persistence of the whole species via periodic or chaotic dynamics, avoiding the extinction of top predators. This result is another example that unstable dynamics (such as chaos) can facilitate species coexistence or survival, as showed by other authors within the frameworks of homeochaotic [29,30] and metapopulation [15] dynamics.

Declaration of Competing Interest

We declare we do not have competing interests

CRediT authorship contribution statement

Ll. Alsedà: Data curation, Formal analysis, Funding acquisition, Investigation, Methodology, Project administration, Resources, Software, Supervision, Validation, Visualization, Writing - original draft, Writing - review & editing. **B. Vidiella:** Data curation, Formal analysis, Investigation, Methodology, Resources, Software, Visualization, Writing - original draft, Writing - review & editing. **R. Solé:** Conceptualization, Funding acquisition, Investigation, Methodology, Project administration, Resources, Visualization, Writing - original draft, Writing - review & editing. **J.T. Lázaro:** Data curation, Formal analysis, Funding acquisition, Investigation, Methodology, Resources, Software, Visualization, Writing - original draft, Writing - review & editing. **J. Sardanyés:** Data curation, Formal analysis, Funding acquisition, Investigation, Methodology, Project administration, Resources, Software, Validation, Visualization, Writing - original draft, Writing - review & editing.

Acknowledgments

The research leading to these results has received funding from “la Caixa” Foundation, from a MINECO grant awarded to the Barcelona Graduate School of Mathematics (BGSMath) under the “María de Maeztu” Program (grant MDM-2014-0445), and from the CERCA Programme of the Generalitat de Catalunya. LlA has been supported by the Spain’s ”Agencial Estatal de Investigación” (AEI) grant MTM2017-86795-C3-1-P. JTL has been partially supported by the Catalan grant 2017SGR1049, by the MINECO grant MTM2015-65715-P, and by grant PGC2018-098676-B-100 (AEI/FEDER/UE). JS has been also funded by a “Ramón y Cajal” Fellowship (RYC-2017-22243) and by a MINECO grant MTM-2015-71509-C2-1-R and the AEI grant RTI2018-098322-B-I00. RS and BV have been partially funded by the Botin Foundation, by Banco Santander through its Santander Universities Global Division and by the PR01018-EC-H2020-FET-Open MADONNA project. RS also acknowledges support from the Santa Fe Institute. JTL thanks the Centre de Recerca Matemàtica (CRM) for its hospitality during the preparation of this work. We also want to thank Sergi Valverde for useful comments.

Supplementary material

Supplementary material associated with this article can be found, in the online version, at doi:10.1016/j.cnsns.2020.105187.

References

[1] Solé R, Bascompte J. Self-organization in complex ecosystems. Princeton University Press; 2006.
[2] Elton CS. Fluctuations in the numbers of animals: their causes and effects. Br J Exp Biol 1924;2:119–63.
[3] Elton CS, Nicholson M, Anim J. The 10-year cycle in numbers of the lynx in canada. Ecol 1924;11:215–44.
[4] Constantino RF, Desharnais RA, Cushing JM, Dennis B. Chaotic dynamics in an insect population. Science 1997;275:389–439.
[5] Dennis B, Desharnais RA, Cushings JM, Constantino RF. Estimating chaos and complex dynamics in an insect population. J Anim Ecol 1997;66:704–29.
[6] May RM. Biological populations with nonoverlapping generations: stable points, stable cycles and chaos. Science 1974;186:645–7.
[7] May RM. Simple mathematical models with very complicated dynamics. Nature 1976;261:459–67.
[8] May RM, Oster GF. Bifurcations and dynamic complexity in simple ecological models. Am Nat 2006;110:573–99.
[9] Schaffer WM, Kot M. Chaos in ecological systems: the coals that newcastle forgot. Trends Ecol Evol 1986;1:58–63.
[10] Gilpin ME. Spiral chaos in a predator-prey model. Am Nat 1979;107:306–8.
[11] Hastings A, Powell T. Chaos in a three-species food chain. Ecology 1991;72:896–903.
[12] Rössler OE. An equation for continuous chaos. Phys Lett A 1976;57:397–8.
[13] Schaffer WM, Math J. Can nonlinear dynamics elucidate mechanisms in ecology and epidemiology? IMA Appl Med Biol 1985;2:221–52.
[14] Berryman AA, Millsten JA. Are ecological systems chaotic ? and if not, why not? Trends Ecol Evol 1989;4:26–8.
[15] Allen JC, Schaffer WM, Rosko D. Chaos reduces species extinction by amplifying local population noise. Nature 1993;364:229–32.
[16] Schaffer WM. Stretching and folding in lynx fur returns: evidence for a strange attractor in nature? Am Nat 1984;124:798–820.
[17] Turchin P. Chaos and stability in rodent population dynamics: evidence from nonlinear time-series analysis. Oikos 1993;68:167–72.
[18] Turchin P. Chaos in microtine populations. Proc R Soc Lond B 1995;262:357–61.
[19] Gamarra JGP, Solé RV. Bifurcations and chaos in ecology: lynx returns revisited. Ecol Lett 2000;3:114–21.
[20] Turchin P, Ellner SP. Living on the edge of chaos: population dynamics of fennoscandian voles. Ecology 2000;81:3099–116.
[21] Benincà E, Huisman J, Heerkloss R, Jöhnk KD, Branco P, Nes EHV. Chaos in a long-term experiment with a plankton community. Nature 2008;451:822–6.
[22] Desharnais RA, Costantino RF, Cushing JM, Henson SM, Dennis B. Chaos and population control of insect outbreaks. Ecol Lett 2001;4:229–35.
[23] Dennis B, Desharnais RA, Cushing JM, Henson SM, Constantino RF. Estimating chaos and complex dynamics in an insect population. Ecol Monogr 2001;7(12):277–303.
[24] Haugen IMA, Berger D, Gotthard K. The evolution of alternative developmental pathways: footprints of selection on life-history traits in a butterfly. J Evol Biol 2012;25. 1388–1388
[25] Hassell MP, Comins HN, May RM. Spatial structure and chaos in insect population dynamics. Nature 1991;353:255–8.
[26] Solé RV, Bascompte J, Valls J. Nonequilibrium dynamics in lattice ecosystems: chaotic stability and dissipative structures. Chaos 1992;2:387–95.
[27] Sardanyés J, Solé R. Red queen strange attractors in host-parasite replicator gene-for-gene coevolution. Chaos, Solitons Fractals 2007;32:1666–78.
[28] Sardanyés J. Low dimensional homeochaos in coevolving host-parasitoid dimorphic populations: extinction thresholds under local noise. Commun Nonlinear Sci Numer Simulat 2011;16:3896–903.
[29] Kaneko K, Ikegami T. Homeochaos: dynamics stability of symbiotic network with population dynamics and evolving mutation rates. Phys D 1992;56:406–29.

[30] Ikegami T, Kaneko K. Evolution of host-parasitoid network through homeochaotic dynamics. Chaos 1992;2:397–407.
[31] McCallum HI, M Schaffer W, Kott M. Effect of immigration on chaotic population dynamics. J theor Biol 1992;154:277–84.
[32] Duarte J, Januário C, Martins N. Topological invariants in the study of a chaotic food chain system. Chaos 2008;18(023109):1–9.
[33] Deng B. Food chain chaos due to junction-fold point. Chaos 2001;11(3):514–25.
[34] Deng B, Hines G. Food chain chaos due to shilnikov's orbit. Chaos 2002;12(3):533–8.
[35] Deng B, Hines G. Food chain chaos due to transcritical point. Chaos 2003;13(2):578–85.
[36] Deng B, Hines G. Food chain chaos with canard explosion. Chaos 2004;14(4):1083–92.
[37] Elsadany AA. Dynamical complexities in a discrete-time food chain. Comp Ecol and Software 2012;2(2):124–39.
[38] Ackleh AS, De Leenheer P. Discrete three-stage population model: persistence and global stability results. J Biol Dyn 2008;2(4):415–27.
[39] Zhang L, Zhao HF. Periodic solutions of a three-species food chain model. Appl Math E-Note 2009;9:47–54.
[40] Lauwerier HA, Holden AV. Two-dimensional iterative maps. chaos. Princeton University Press; 1986. 58-95
[41] Vidiella B, Alsedà L, Lázaro JT, Sardanyés J. On dynamics and invariant sets in predator-prey maps. Dynamical Systems Theory. Awrejcewicz J, editor. IntechOpen; 2019.
[42] Kon R, Takeuchi Y. The effect of evolution on host-parasitoid systems. J theor Biol 2001;209:287–302.
[43] KhSaulich A, Musolin DL. Seasonal cycles in stink bugs (*Heteroptera, Pentatomidae*) from the temperate zone: diversity and control. Enthomol Rev 2014;94:785–814.
[44] Parker T, Chua LO. Practical numerical algorithms for chaotic systems. Berlin: Springer-Verlag; 1989.
[45] Schuster HG. Deterministic chaos: an introduction. Weinheim: Physik-Verlag; 1984.
[46] Kuznetsov YA. Elements of applied bifurcation theory. New York: Springer-Verlag; 1998.
[47] Kim J-I, Park H-K, Moon HT. Period doubling of a torus: chaotic breathing of a localized wave. Phys Rev E 1997;55(4):3948–51.
[48] Arnéodo A, Coullet PH, Spiegel EA. Cascade of period doublings of tori. Phys Lett A 1983;94(1):1–6.
[49] Letellier C, Bennoud M, Martel G. Intermittency and period-doubling cascade on tori in a bimode laser model. Chaos, Solitons Fractals 2007;33(3):782–94.